https://doi.org/10.5194/egusphere-2025-1212
Preprint. Discussion started: 25 March 2025

Parameterization adaption needed to unlock the benefits of increased resolution for the ITCZ in ICON

Clarissa A. Kroll[1], Andrea Schneidereit[2], Robert C. J. Wills[1], Luis Kornblueh[3], and Ulrike Niemeier[3]

[1]Institute for Atmospheric and Climate Science, ETH Zürich, Zürich, Switzerland
[2]Deutscher Wetterdienst, Offenbach am Main, Germany
[3]Max Planck Institute for Meteorology, Hamburg, Germany

Correspondence: Clarissa A. Kroll (clarissa.kroll@env.ethz.ch)

Abstract. The double Inter-Tropical Convergence Zone (dITCZ) is a prominent precipitation bias persistent over several climate model generations. This motivates investigations of whether increasing resolution and discarding parametrizations can improve the representation of the large-scale atmospheric circulation. In this work, we use the unique possibility offered by the new ICON XPP model configuration to study the dITCZ bias in a resolution hierarchy spanning from parameterized to resolved convection within a consistent modeling framework. We demonstrate that the dITCZ persists from a horizontal resolution of 160 km up to 5 km in specified sea surface temperature simulations and is independent of the deep-convective and non-orographic gravity wave parametrization. Changes in the treatment of near-surface wind speed within the bulk flux formula can reduce the dITCZ bias over the resolution hierarchy. We however highlight that the root cause of the dITCZ lies in biased moisture transport from the subtropics to the inner tropics. The resulting low bias in tropical near-surface moisture substantially reduces deep convection over the Warm Pool, leading to a weakened Walker Circulation. These biases ultimately culminate in the dITCZ feature. An increase in near-surface wind speed addresses the low bias in near-surface moisture in the tropics, however it exacerbates a bias in the moisture source by increasing the inner tropical over the subtropical contribution. This could endanger the representation of the global circulation, energetic balance and teleconnections. Our findings showcase the benefits of models supporting a range of resolutions and underline the importance of continuing the development of non-discardable parametrizations.

1 Introduction

The hydrological cycle is an important manifestation of the global atmospheric circulation and plays a key role in Earth's energy budget. The Inter-Tropical Convergence Zone (ITCZ) is at the center of the meridional circulation which imports moisture into the tropics and exports energy to higher latitude (Holton, 2004; Schneider et al., 2014). Despite its importance, biases in the representation of precipitation within the ITCZ have been a persistent challenge throughout model generations in the Coupled Model Intercomparison Project, CMIP(Tian and Dong, 2020). Among them, the double-ITCZ bias (dITCZ), i.e., the tendency to overestimate precipitation over ocean in the southern tropics and underestimate it at the equator, is the most prominent problem. Since the impacts of the double-ITCZ are relevant beyond the ocean regions in which it occurs, influencing the El Niño-Southern Oscillation and other large-scale climate phenomena(Ham and Kug, 2014; Zhang et al., 2014), the origin of

https://doi.org/10.5194/egusphere-2025-1212
Preprint. Discussion started: 25 March 2025

this bias has been central to the precipitation bias discussions.

When speaking of the dITCZ, it is important to note that the dITCZ is not an entirely artificial phenomenon which is only seen in climate simulations. In fact observations indicate the dITCZ can also occur naturally at certain times of the year, preferentially in March. The problem is therefore not the appearance of the dITCZ as such but that it is too strong and persists throughout the year in model simulations. Over the Pacific, the natural dITCZ feature is associated with local minima in surface humidity and temperature along the equator (Zhang, 2001) or increased wind convergence (Halpern and Hung, 2001).

In order to understand the simulated year-long dITCZ bias, the role of the ITCZ in the earth system has to be studied. The ITCZ is part of the global system of energy redistribution, which in the atmosphere is largely handled by the large-scale meridional circulation. Subtropical moisture is transported within the Trade Winds into the inner tropics, fueling the hydrological cycle. This supply of moisture from higher latitudes leads to the well-known excess of precipitation over evaporation caused moisture mass flux in the tropics. The moisture import into the tropics is then balanced by an energy export to the subropics, with the ITCZ at the center of the corresponding meridional circulation, the Hadley cells. Since the position and structure of the ITCZ and distribution of net energy input to the atmosphere are interrelated (Bischoff and Schneider, 2014; Ren and Zhou, 2024), changes in the distribution of precipitation will be reflected in the atmospheric energy budget, and vice versa. For example, the ITCZ resides in the Northern Hemisphere in the annual-mean due to the difference in the net energy input between the Northern and Southern Hemispheres (Philander et al., 1996). In an energetically motivated framework, precipitation biases can be separated into hemispherically symmetrical and asymmetrical components (Hwang and Frierson, 2013; Adam et al., 2016). The symmetric component is related to the net energy input near the equator and the anti-symmetric component to cross-equatorial energy flux, which again is influenced by asymmetries in the net energy input in the two hemispheres. This underlines that the dITCZ problem cannot be investigated as an isolated tropical phenomenon, since subtropical biases in the energy budget can also be sources of the problem (Kang et al., 2008; Hwang and Frierson, 2013), and tropical biases can likewise cause biases in the subtropics (Dong et al., 2022).

This coupling between the dITCZ problem and biases in the energy budget is critical in recognizing in the context of model tuning, because the first model evaluation step is – most naturally – the energy balance of the model (Wild, 2020). Most model evaluation workflows focus first on global mean top-of-the-atmosphere (TOA) fluxes and potentially surface energy fluxes (Mauritsen et al., 2012), with the understanding that modelers will then tune additional atmospheric fields and processes, for example, as outlined in Hourdin et al. 2017 (Hourdin et al., 2017). However, most published model evaluation workflows provide little information on the regional energy budgets that are mechanistically important for the large-scale circulation and the distribution of precipitation. This poses a problem: sometimes improvements in global-mean energy fluxes introduce compensating errors in regional energy fluxes and lead to deterioration of the large-scale circulation and precipitation distribution.

Next to model tuning choices which disregard the impact on the large-scale circulations, an additional possible source of tropical precipitation biases is the incorrect representation of convective processes in coarse-scale models. Discarding potentially

https://doi.org/10.5194/egusphere-2025-1212
Preprint. Discussion started: 25 March 2025

error-prone convective parametrizations (Jones and Randall, 2011; Sherwood et al., 2014) has therefore been one of the avenues explored to address this problem (Arakawa, 2004; Hardiman et al., 2015; Song and Zhang, 2018; Ma et al., 2023). In this context, it is important to note that although it is often stated that high-resolution simulations are less sensitive to parametrization choices than low-resolution simulations, some parametrizations still remain – such as the microphysics, non-orographic gravity wave, turbulence, and in some cases shallow convective parametrizations – all of which are of importance for the model energetics (Hu et al., 2021; Hájková and Šácha, 2023). High computational costs, in combination with the misconception that all relevant processes are now resolved, often lead to a substantial shortening of the model tuning process in high-resolution simulations. Therefore, the lack of systematic tuning could be one of the reasons why high-resolution convection-resolving simulations without parametrizations do not show improvements in skill for the tropical precipitation pattern compared to conventional CMIP models, whereas high-resolution simulations still relying on parametrization can outperform both (Zhou et al., 2022; Schneider et al., 2024).

In this work, we investigate the precipitation distribution and the dITCZ bias in a resolution hierarchy of the ICON model spanning from parametrization supported 160 km to deep-convection resolving 5 km horizontal resolution. We outline the influence of modeling parameter choices over the resolution hierarchy, using an otherwise identical setup, model code, and boundary conditions, to allow for a robust and fair comparison. This endeavor has only recently been made possible within the ICON XPP configuration (Früh et al., 2022; Niemeier et al., 2023; Müller et al., 2024) which in contrast to ICON sapphire (Hohenegger et al., 2022) supports the usage of convective parametrizations in ICON. We focus on three leading questions:

1. Can increased horizontal resolution and the discard of deep convective and gravity wave parametrization resolve the dITCZ bias? Are there common biases across resolutions? Where can resolution-dependent improvements be found? (*Addressed in Section 3.1*)

2. To the extent that there are common (dITCZ) biases, how can they be addressed and can the same adjustments be applied at various resolutions?
(*Addressed in Section 3.2 and 3.3*)

3. What are the underlying mechanisms leading to the dITCZ biases and how do the chosen adjustments ameliorate it? (*Addressed in Section 3 and Section 4, summarized in Fig 13*)

To address the second research question, we focus on the choice of a minimum surface wind speed threshold in the bulk-flux formulation. Mechanistically, following the bulk flux formula, a higher U_{min} leads to an increased latent heat flux into the atmosphere in low-wind conditions, and with it more available moisture for convection, the fuel for the hydrological cycle. The minimum wind speed limiter is particularly interesting for a resolution study as it is not only known to be a promising tuning candidate (Segura et al., 2024) but it may also be resolution dependent, with generally more vehement winds at increased horizontal resolution (Jeevanjee, 2017; Iles et al., 2020; Paccini et al., 2021; Morris et al., 2024). The surface wind speed limiter is an example for a “minor-looking treatment" where the lower or upper boundaries of physical parameters are restricted. As

https://doi.org/10.5194/egusphere-2025-1212
Preprint. Discussion started: 25 March 2025

"minor-looking treatments" can have impacts comparable to the exchange of parameterization schemes (Kawai et al., 2022), their implementation should receive more attention.

95

In the following, we will show that precipitation biases are reduced with increases in resolution and with an increase in the minimum surface wind speed threshold, both in the large-scale precipitation field and a simplified ITCZ metric. Then we discuss the underlying physical mechanisms of this improvement, including additional focus on the trade-offs of the improved precipitation bias for other key quantities, which we proceed to retune in coarse resolution. In a last step, the transferability
100 of the gained knowledge with respect to tuning choices to higher resolution is tested. We also outline why our experiments hint that the actual root cause for the precipitation biases does not reside in the tropics but in the outer and subtropics. For this purpose we contrast the real world atmospheric representation and energy distribution, the one simulated by ICON expressing a dITCZ and the one one simulated by ICON with surface wind limiter adjustments. The identified large-scale differences in the three scenarios are summarized at the end of the work. The reader might find it helpful to refer to the schematic found there
105 throughout the text.

2 Methods

2.1 Model simulations

2.1.1 Model setup

Simulations are performed with the atmosphere model of the Icosahedral Nonhydrostatic Weather and Climate Model for
110 Numerical Weather Prediction, ICON-NWP (Zängl et al., 2015; Prill et al., 2023), in the eXtendedPrediction and Projection, XPP-configuration[1] (Früh et al., 2022; Niemeier et al., 2023; Müller et al., 2024). ICON XPP uses the parametrizations for radiation ecRad (Hogan and Bozzo, 2018), microphysics (Seifert, 2008), turbulent transfer (TKE, Raschendorfer (2001)), convection (Tiedtke, 1989; Bechtold et al., 2008), sub-grid scale orographic drag (Lott and Miller, 1997) and non-orographic gravity wave drag (Orr et al., 2010) together with the JSBACH land model (Reick et al., 2021).

115

Simulations are carried out in a hierarchy of four horizontal resolutions: R2B4, 160 km; R2B5, 80 km; R2B6, 40 km and R2B9, 5 km. This covers the horizontal resolution of conventional CMIP-type models (160 km) up to the resolution of deep-convection resolving models (5 km). The 80 km and 40 km serve as some additional intermediate resolution steps to test for the impact of i.e. improved orographic representation. For all resolutions, 150 vertical levels up to a model top of 75 km are employed with a
120 constant layer thickness of 300 m from a height of 8.4 km to 19 km to fully capture the altitude range of deep convection, even in the inner tropics (Schmidt et al., 2023). For the 5 km simulations, the parameterization for sub-grid non-orographic gravity waves, mid-level and deep convection are disabled following the ICON sapphire protocol (Hohenegger et al., 2022), however, the orographic gravity wave drag and shallow-convective parameterization are kept, as in the general numerical weather fore-

[1]Formerly: Seamless configuration

https://doi.org/10.5194/egusphere-2025-1212
Preprint. Discussion started: 25 March 2025

casting protocol.

2.1.2 Experiments

For all coarser horizontal resolutions, control simulations – CTL-R2B4, CTL-R2B5 and CTL-R2B6 – are run for six years using climatological sea ice and sea surface temperature fields from the CMIP6 Forcing Datasets (input4MIPs, 1978-2020) as boundary conditions (Durack and Taylor, 2018). The usage of prescribed, climatological SSTs reduces the impact of interannual variability such as the influence of ENSO-events on the precipitation. Branching off at the fourth year of these simulations, two-year-long sensitivity studies (perturbed, from here on PTB) are performed in R2B6, varying the minimum surface wind speed limiter, U_{min}, presented to the turbulence scheme (Table 1). Specifically, this limiter is set as the squared velocity input $\boldsymbol{U}^2_{total} = U^2_{min}$ for the wind shear term of the near-surface moist Richardson number if the squared horizontal velocities with gustiness correction meets the criterion $\boldsymbol{U}^2_{total} < U^2_{min}$. This means that surface fluxes are determined in dependence of U_{min} in cases where the actual grid-scale wind speed is less than U_{min}. This method has been used to account for the influence of sub-grid-scale turbulence.

For the two settings performing best in representing the large-scale annual-mean ITCZ, PTB-5 and PTB-6, with $U_{min} = 5ms^{-1}$ and 6 ms^{-1}, respectively, the wind speed is optimized for land and ocean separately (PTB-5_1 and PTB-6_1, indicating that $U_{min} = 1ms^{-1}$ over land) followed by model retuning (PTB-5_1t, PTB-6_1t) to reestablish the CTL top-of-the-atmosphere (TOA) imbalance.

Due to the exceptionally high computation demand, the CTL-R2B9 is run for three years instead of the six years of the coarser simulations. Subsequent to the coarse scale tuning, the best untuned (PTB-5_1) and corresponding tuned settings (PTB-5_1t) are applied to branches off of the CTL-R2B9 simulation for MAM, the key season for the dITCZ representation, to test the validity of the tuning approach throughout the set of horizontal resolutions. To allow the model time to equilibrate to the changed settings a one month spin-up is used.

As the investigated horizontal resolutions differ by up to a factor of 32, all data sets are remapped for a fair comparison in the subsequent analysis. For this purpose, a 1 degree horizontal resolution is chosen, which is near to the tropical 1.4 degree horizontal resolution of the coarsest simulation, R2B4, with uniform 160 km horizontal grid spacing.

2.2 Reference: reanalysis and observational data sets

The model output is evaluated against reanalysis and observational data sets. For the radiative fluxes, data from the Clouds and the Earth's Radiant Energy System, CERES (Doelling et al., 2013, 2016), an observational data set for TOA energy fluxes, is used. The precipitation distribution is compared to the observational data sets Integrated Multi-satellitE Retrievals

https://doi.org/10.5194/egusphere-2025-1212
Preprint. Discussion started: 25 March 2025

Table 1. Summary of Experiments: Experiment acronyms, employed resolutions, simulated timeframe, setting for the minimum horizontal wind speed over ocean/land and tuning. The Control simulation (CTL) run for all resolutions is marked in gray, the best-performing perturbed experiment (PTB) for the ITCZ representation is marked in green.

Experiment	Resolution	Simulated Timeframe	Surface Wind Speed Limiter U_{min} (Ocean/Land) / ms^{-1}	Tuned
PTB-0.5	R2B6	2 years	0.5 / 0.5	
CTL	R2B{4,5,6}	6 years	1.0 / 1.0	✓
	R2B9	3 years	1.0 / 1.0	✓
PTB-1.5	R2B6	2 years	1.5 / 1.5	
PTB-2	R2B6	2 years	2.0 / 2.0	
PTB-4	R2B6	2 years	4.0 / 4.0	
PTB-5	R2B6	2 years	5.0 / 5.0	
PTB-5_1	R2B6	2 years	5.0 / 1.0	
PTB-5_1	R2B9	2 MAM	5.0 / 1.0	
PTB-5_1t	R2B6	2 years	5.0 / 1.0	✓
	R2B9	2 MAM	5.0 / 1.0	✓
PTB-6	R2B6	2 years	6.0 / 6.0	
PTB-6_1	R2B6	2 years	6.0 / 1.0	
PTB-6_1t	R2B6	2 years	6.0 / 1.0	✓

for GPM (IMERG, Huffman et al. (2010)) and Global Precipitation Climatology Project (GPCP, Huffman (2021)). In addition to these observational data sets, we show radiative fluxes from the fifth generation ECMWF atmospheric reanalysis (ERA5, Hersbach et al. (2017); C3S (2018); Simmons et al. (2020)), noting that these values are not assimilated, which means that the reanalysis product might behave more like a conventional model here and should only be used as complementing the ground truth observational data. For latent heat flux, near-surface wind speeds and near-surface specific humidity q_s we refer to ERA5 as primary reference as it assimilates station-based humidity measurements (Simpson et al., 2024) and offers a homogeneous data set with values both over land and ocean. Whereas latent heat flux and near-surface wind speeds are direct outputs of ERA5, the values of q_s are derived via

$$q_s = \frac{0.622\, p_v}{p_s - 0.378\, p_v}. \tag{1}$$

using the vapour pressure p_v in hPa, which is calculated using ERA5 output of 2-m dew point temperature T_D in Celsius and surface pressure p_s in hPa according to the Magnus formula

$$p_v = 6.112 \times 5 \exp\left(\frac{17.67 T_D}{T_D + 243.5\,\mathrm{K}}\right). \tag{2}$$

https://doi.org/10.5194/egusphere-2025-1212
Preprint. Discussion started: 25 March 2025

In order to assess biases in the ERA5 latent heat flux values a comparison to the OAFlux data set (Fairall et al., 2003; Yu and Weller, 2007; Schneider et al., 2013; National Center for Atmospheric Research Staff, 2022), which integrates satellite retrievals and three atmospheric analyses, is made.

2.3 ITCZ evaluation metrics

To evaluate the bulk ITCZ features, we use an energetically-motivated framework. Here, precipitation biases can be separated into hemispherically symmetric and antisymmetric components (Hwang and Frierson, 2013; Adam et al., 2016). The symmetric component

$$E_p = \frac{\overline{P}_{2^\circ S-2^\circ N}}{\overline{P}_{20^\circ S-20^\circ N}} - 1 \tag{3}$$

is related to the net energy input near the equator where $E_p = 0$ would describe a state where the precipitation average between 2° South and 2° North is equal to the precipitation average between 20° South and 20° North. The anti-symmetric component

$$A_p = \frac{\overline{P}_{0N-20^\circ N} - \overline{P}_{0^\circ S-20^\circ S}}{\overline{P}_{20^\circ S-20^\circ N}}, \tag{4}$$

is related to the cross-equatorial energy flux, which is influenced by asymmetries in the net energy input in the high latitudes of the two hemispheres. $\overline{P}$ is the precipitation averaged over the region constrained by the two latitude boundaries referred to in the respective subscript.

3 Results

3.1 Consistent large-scale precipitation biases across horizontal resolutions

To address research question 1, we test if the increase in horizontal resolution and discard of parametrizations reduces the dITCZ bias and investigate where the model resolution has an impact on the model biases. Our analysis of the yearly-averaged precipitation shows qualitatively similar biases compared to IMERG data in all four resolutions of ICON (Fig. 1). Quantitatively, there is a consistent improvement in the global root mean square error (RMSE) with respect to IMERG from 1.55 mm day^{-1} (R2B4, 160 km) to 1.27 mm day^{-1} (R2B9, 5 km)[2]. Areas of consistent improvement include coastal regions, e.g., in the ITCZ on either side of South America, and over tropical land, where benefits could partially arise from the improved representation of topographic features. This is particularly true for some of the islands in the Western Pacific Warm Pool, which show a considerable decrease in the dry precipitation bias in the 5 km simulations.

[2]Fig.A1 depicts the significance threshold for a two sided z-test at α=0.1. All major tropical deviations are significant and not marked for better visualization in Fig. 1.

https://doi.org/10.5194/egusphere-2025-1212
Preprint. Discussion started: 25 March 2025

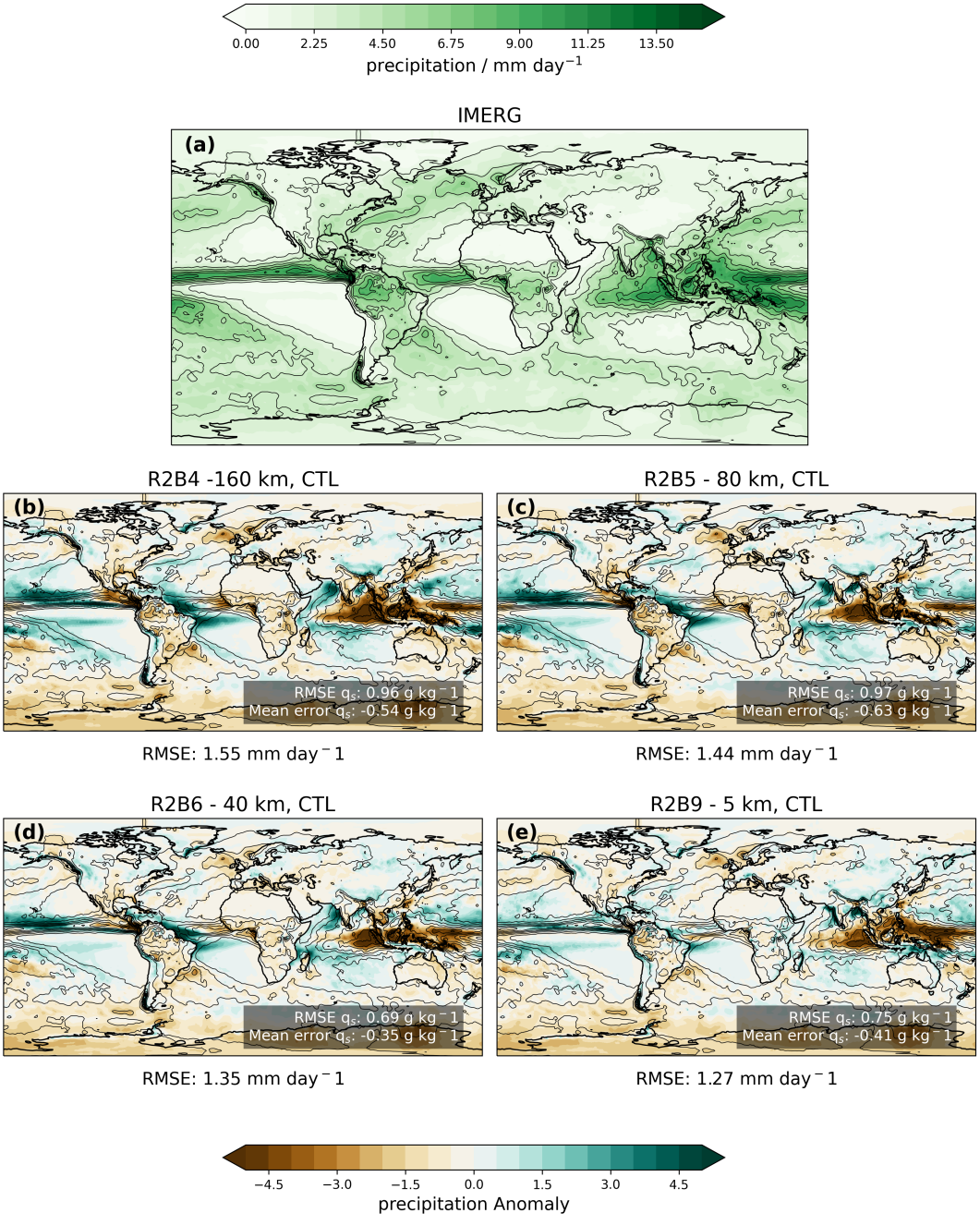

Figure 1. Climatological IMERG precipitation distribution from 2004 to 2010 and two-year mean precipitation bias with respect to IMERG for R2B4 (160 km), R2B5 (80 km), R2B6 (40 km) and R2B9 (5 km) setups. Contours show the IMERG climatology. The corresponding global RMSE in precipitation is stated beneath the panel for each resolution experiment. The global RMSE and mean error in near-surface specific humidity calculated with respect to values derived from ERA5 reanalysis is depicted in the inlays.

https://doi.org/10.5194/egusphere-2025-1212
Preprint. Discussion started: 25 March 2025

On the large-scale however, all resolutions show the same regions of precipitation biases. Especially apparent in the tropics are the dITCZ feature over the Pacific and Atlantic as well as the dry bias over the Maritime Continent East Asia, the prominent tropical convective region. The dry bias in the West Pacific and wet biases in the East Pacific hint that the westward transport of boundary layer moisture within the zonally anomalous Walker Circulation is too weak. The tropical dry bias over the Warm Pool is tied to a lack of near-surface specific humidity throughout the entire tropics (average global scores in inlays of Fig. 1; spatial distribution in Appendix Fig. B1). The lack of near-surface specific humidity impacts the vertical moisture distribution and inhibits the build-up of larger deep convective systems in the inner tropics (Fig. 2). Consistent for all resolutions, the regions between 20° S and 20° N are too dry below 1 km in altitude. In the 80 km and 5 km simulations, the dry region extends to even higher latitudes in the North. The lack of boundary-layer moisture in the inner tropics is reflected in the innermost tropical free troposphere. In contrast to the inner tropics, the areas between 15° to 40 ° North resp. South exhibit a moist bias above 1 km in height, peaking at around 20 degrees at a height of 2 km.

https://doi.org/10.5194/egusphere-2025-1212
Preprint. Discussion started: 25 March 2025

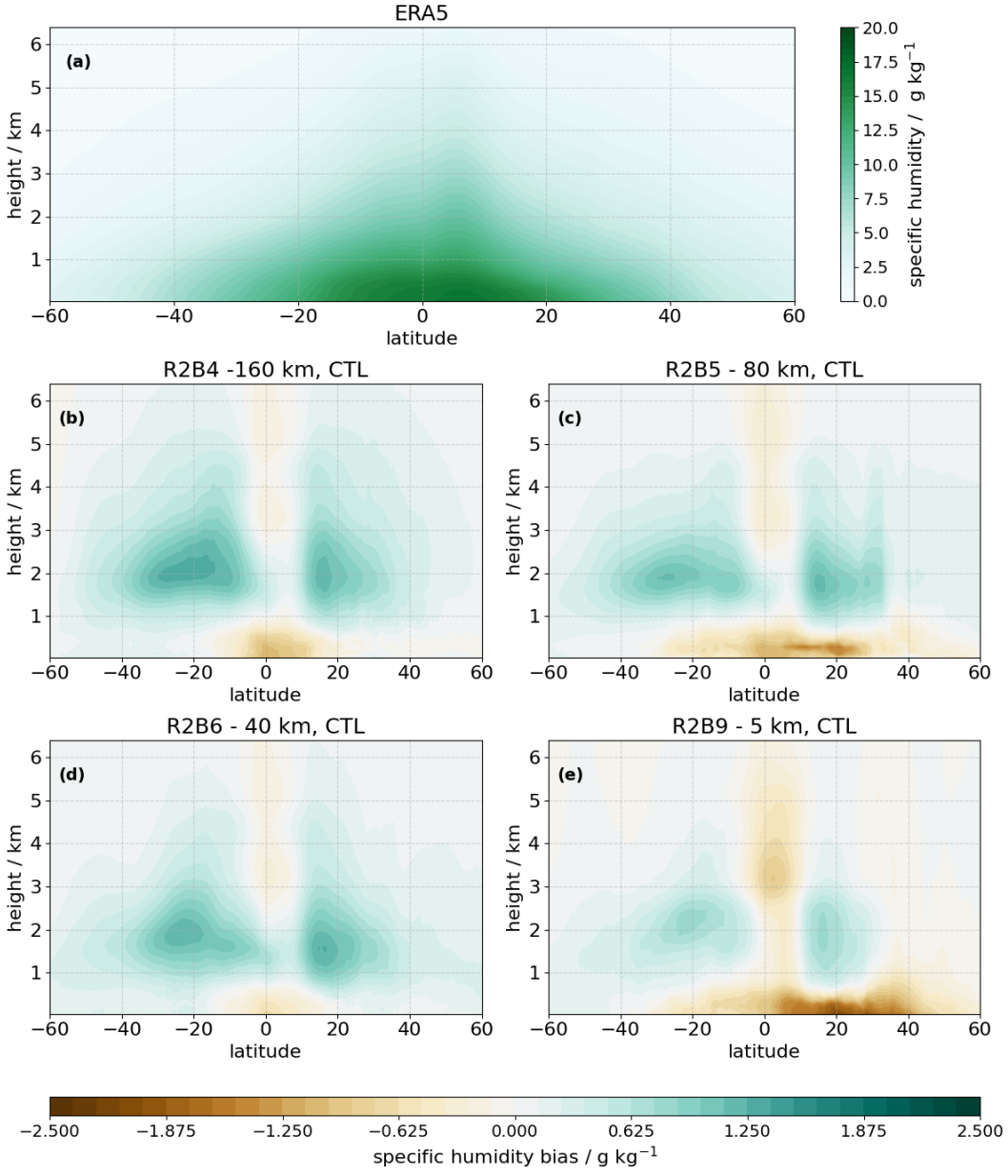

Figure 2. Climatological zonal-mean atmospheric specific humidity distribution from ERA for the years 2004 to 2010 and two-year atmospheric specific humidity bias with respect to ERA5 for R2B4 (160 km), R2B5 (80 km), R2B6 (40 km) and R2B9 (5 km) setups.

The consequences of the biases in the humidity distribution are also apparent in the zonal mean temperature biases (Fig 3, cf. Fig 2). Across the resolutions a similar picture persists: a near-surface warm bias and a cold bias in the free troposphere. An exception is the region around 20-40° N, where the near-surface warm bias extends upwards to higher atmospheric layers. The near-surface warm bias is most likely caused by the dry bias in the near surface layer which ties the atmosphere closer to a dry

https://doi.org/10.5194/egusphere-2025-1212
Preprint. Discussion started: 25 March 2025

adiabatic lapse rate which leads to a warming of the near-surface atmosphere and cooling of the free troposphere aloft. The other findings are consistent with Fig. 1 and Fig. 2: The cold bias in the tropical free troposphere is consistent with the reduced deep convection over the Warm Pool. The missing latent heating in the free troposphere leads to a cooler atmosphere or in other words the near-surface dry bias will cause the convection to tie the temperature profile nearer to a dry adiabat. As temperatures in the tropics are quite homogeneous, as explained by the Weak Temperature Gradient theory **?**Held and Hoskins (1985), this bias propagates through the tropical region. The band of warm air at 20-40° N collocates with the region influenced by the local topography of the Himalaya. Winds following the terrain are directed upwards, advecting tracers and heat Pan et al. (2016). The general free tropospheric temperature bias improves with increasing resolution up to 40 km deteriorating again at 5 km. As the same tuning was used for 40 km and 5 km, this break in bias trend is most likely caused by the discard of the deep convective parametrizations. As simulations with convective parametrizations are know to create a more stable atmospheric temperature profile than their counterparts without convective paraemtrizations Keil et al. (2021), the relatively cooler free troposphere in R2B9 is an expected finding.

https://doi.org/10.5194/egusphere-2025-1212
Preprint. Discussion started: 25 March 2025

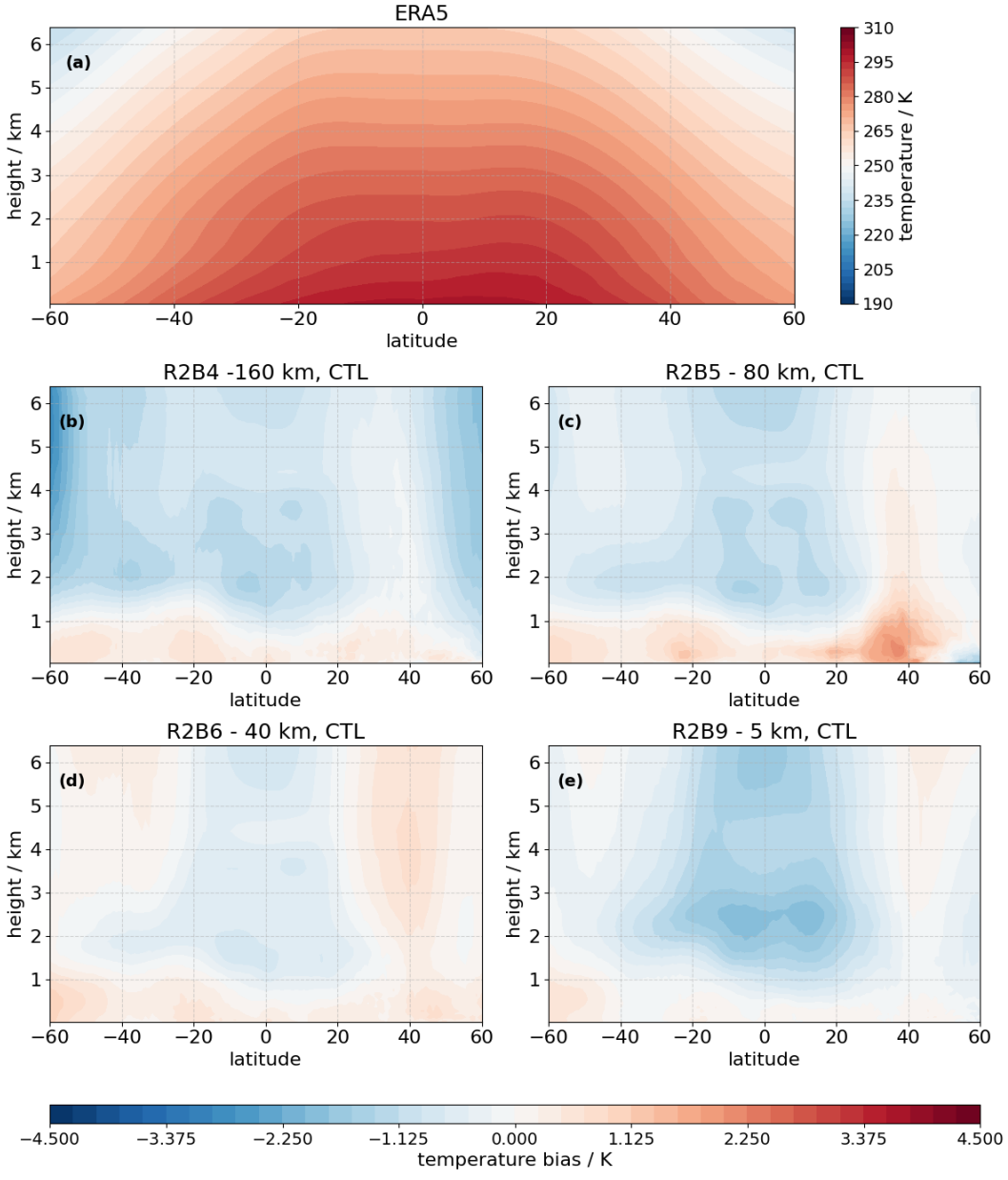

Figure 3. Climatological ERA5 zonal temperature fields averaged over the timeframe from 2004 to 2010 and two-year atmospheric temperature bias with respect to ERA5 for R2B4 (160 km), R2B5 (80 km), R2B6 (40 km) and R2B9 (5 km) setups.

Summarizing the findings to the first research question, we found that increased resolution and discard of parametrizations does not resolve the dITCZ bias up to a resolution of 5 km. Although improvements can be found in the precipitation pattern, especially in orographically complex regions, similar large-scale biases persist. From these biases we gain a first mechanistic understanding of the underlying problem: It appears that the negative bias in near-surface specific humidity is one of the causes

https://doi.org/10.5194/egusphere-2025-1212
Preprint. Discussion started: 25 March 2025

of the precipitation bias. An increase in near-surface moisture would enhance deep convection in the Warm Pool and strengthen the Walker Circulation. A stronger Walker Circulation would increase moisture transport from the East Pacific to West Pacific and further amplify the Walker circulation through a feedback loop. Additionally, the deep convection would lead to a warming of the free troposphere, which would increase the temperature inversion in remote regions, including the Eastern Pacific, which potentially would lead to an additional feedback reinforcing the strengthened circulation, by enhancing the cloud cover in the subsidence regions. The differences between observations and ICON results are conceptually summarized in the schematic at the end of the text.

3.2 Sensitivity of large-scale precipitation biases to the surface wind threshold in the turbulence scheme

With the understanding of the common biases and their potential role in the ITCZ formation, we now focus on the second research question of how to adjust the parameters to counterbalance the found issues in the atmospheric representation. A potential lever is to address the near-surface humidity dry bias over the Warm Pool region. This would interrupt the vicious circle of biases outlined in the previous paragraph. Here, the Bulk Flux Formula

$$E = \rho_a C_E U (q_s - q_a) \tag{5}$$

which ties the evaporation E to wind speed U, near-surface specific humidity q_s, atmospheric specific humidity q_a, atmospheric density ρ_a and a proportionally constant C_E, suggest an increase in horizontal wind speed low-limiter, U_{min}, as a potential lever to address the dry bias over the Warm Pool and the related dITCZ biases, because it would increase the U used to compute the near-surface Richardson number and increase surface fluxes in low-wind regimes, e.g., in the Warm Pool.

In a sensitivity study, performed with the 40 km resolution configuration, we therefore vary U_{min} in the turbulence scheme to evaluate if it improves the dITCZ bias and the dry bias in the Warm Pool region. As the mean near-surface-wind speed in the tropics is lower than in the extratropics (Fig. 5), increases in U_{min} will have a stronger effect in the tropical region. Starting from the default 1 m s^{-1} setting in the CTL simulation, we change U_{min} to the values of $\{0.5, 1.5, 2, 4, 5, 6\}$ m s^{-1}.

https://doi.org/10.5194/egusphere-2025-1212
Preprint. Discussion started: 25 March 2025

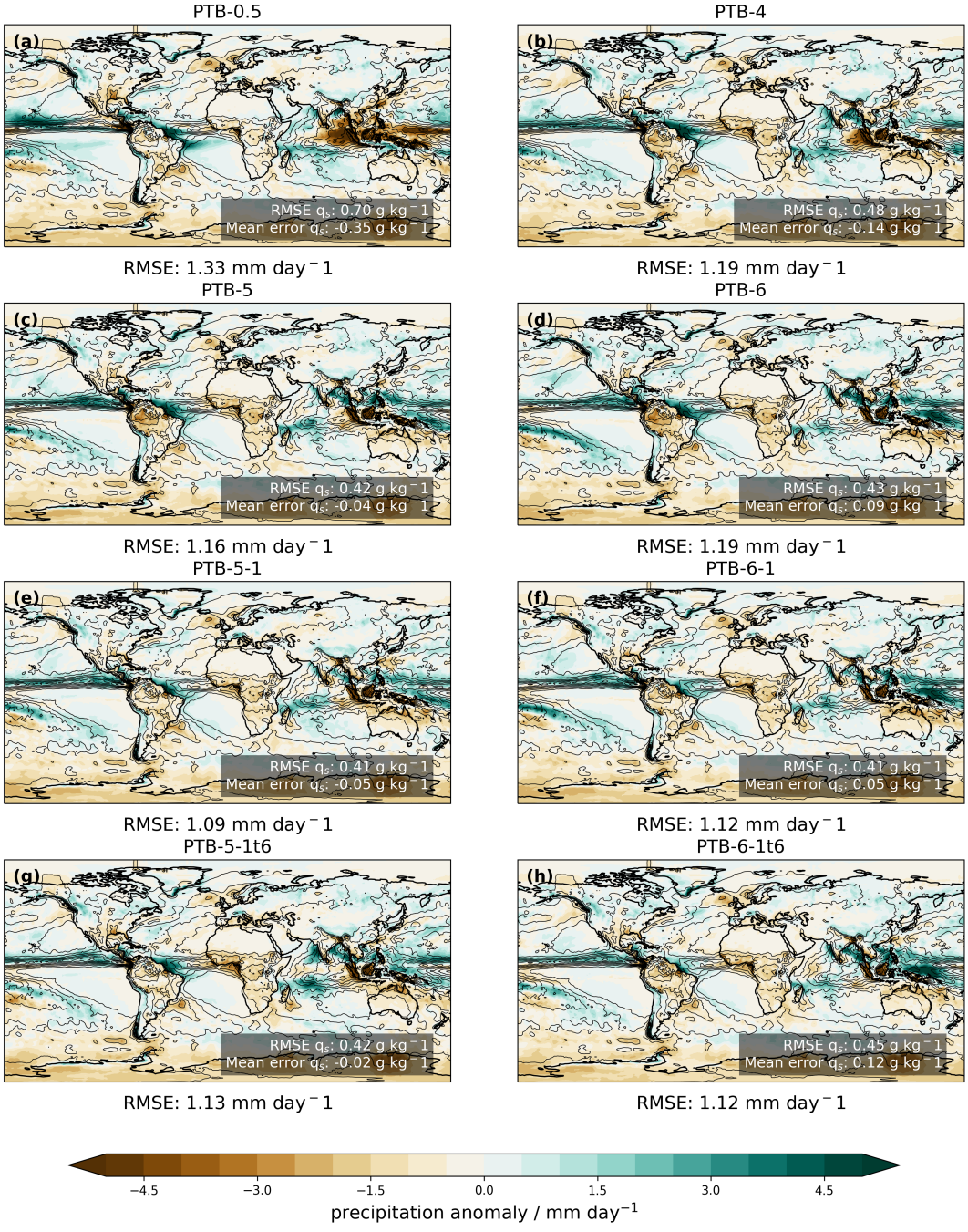

Figure 4. Two-year mean large-scale precipitation bias with respect to IMERG 2004-2010 for different settings of the surface wind in R2B6 (40 km) : PTB-0.5, PTB-4, PTB-5, PTB-5_1, PTB-5_1t, PTB-6, PTB-6_1 and PTB-6_1t. Contours show the IMERG climatology. The corresponding global precipitation RMSE is stated beneath the panel for each sensitivity experiment. The global RMSE and mean error in near-surface specific humidity calculated with respect to values derived from ERA5 reanalysis is depicted in the inlays.

https://doi.org/10.5194/egusphere-2025-1212
Preprint. Discussion started: 25 March 2025

The resulting two-year mean precipitation biases against IMERG are shown in the first two rows of Fig. 4. Indeed the RMSE, both in precipitation and near-surface specific humidity, decreases with increasing threshold in surface wind speed up to a $5\,\mathrm{m\,s^{-1}}$ (PTB-5). Going beyond this value increases the RMSE in precipitation again and a positive precipitation bias develops over the Warm Pool (PTB-6). Although the large-scale precipitation bias, i.e., the dry bias over the Warm Pool and the spurious precipitation band in the South Eastern Pacific disappears, precipitation biases over land remain. Most apparent is the persistent dry bias over the topographically more complex islands in the Warm Pool region, but also a deterioration of the precipitation fields over South America and Africa, which develop an increasing dry bias as U_{min} is increased. We select PTB-5 and PTB-6 as promising candidates for further optimization.

Observational data suggests average wind speed of below $2.5\,\mathrm{m\,s^{-1}}$ at the surface over land, whereas the lower surface roughness over ocean allows for higher wind speeds than over land, with values of 6-7 $\mathrm{m\,s^{-1}}$ (cf. Fig. 6). High values of U_{min} would therefore cut off more of the velocity distribution over land, leading to a problematic lack of sensitivity of land evaporation to wind speed variations, as well as potentially too large surface drag. In the next experiments, we therefore distinguish between ocean and land when setting U_{min}, going back to the CTL setting of $1\,\mathrm{m\,s^{-1}}$ for land in PTB-5_1 and PTB-6_1. This more realistic depiction of the surface wind speeds reverses the increasing dry bias over South America and improves the RMSE precipitation score even further, with PTB-5_1 still outperforming PTB-6_1 (cf. Fig. 4 (e) and (f)).

Although the precipitation distribution improves with the changes in U_{min}, there are some concerns that it might detrimentally affect the velocity distribution as already mentioned above. The physical reasoning behind this is that U_{min} leads to an increase in the wind shear term used for the calculation of the Richardson number reducing its magnitude. The smaller Richardson number leads to a less stable atmosphere, enhanced mixing and consequently to an increase of the surface drag coefficient acting on the near surface velocities. An inspection of the spatially resolved wind fields of CTL, PTB-5, PTB-5_1, PTB-6 and PTB-6_1 compared to ERA5 in Fig. 5 however demonstrates that the impact of changes in the U_{min} is more complicated. As already seen in the precipitation distribution, the mean impact over land and ocean even goes in opposite directions. The choice of unphysical U_{min} values in PTB-5 and PTB-6 leads to an overall reduction in wind speeds over land as U_{min} impacts the momentum fluxes by artificially increasing the surface drag as outlined above. This reduction in overall wind speed above land compared to CTL is reverted when separate U_{min} values are chosen for land and ocean (PTB-5_1, PTB-6_1, PTB-5_1t, PTB-6_1t). In contrast to the surface wind speeds over land (Fig. 5), the surface wind speeds over ocean show a more varied picture. Wind speeds increase in the inner tropics and the Walker Circulation strength, which is too weak in CTL, increases in all perturbation experiments. The perturbation experiments also show improvements in the Northern Hemisphere Trades. Here, the increased moisture supply fueling deep convection and with it the Walker Circulation strength seems to outweigh the increase in surface wind drag. However, other regions where circulations do not depend so much on the additional moisture supply show the expected circulation slow down. For example, a general slowdown of the Trades in the Southern Hemisphere, e.g., off the West Coast of South-America can be noted in all PTB experiments. This not only impacts the moisture transport within in the Trades ranging from 30 to the inner tropics but may also interfere with the wind-evaporation-SST feedback and

https://doi.org/10.5194/egusphere-2025-1212
Preprint. Discussion started: 25 March 2025

related teleconnections.

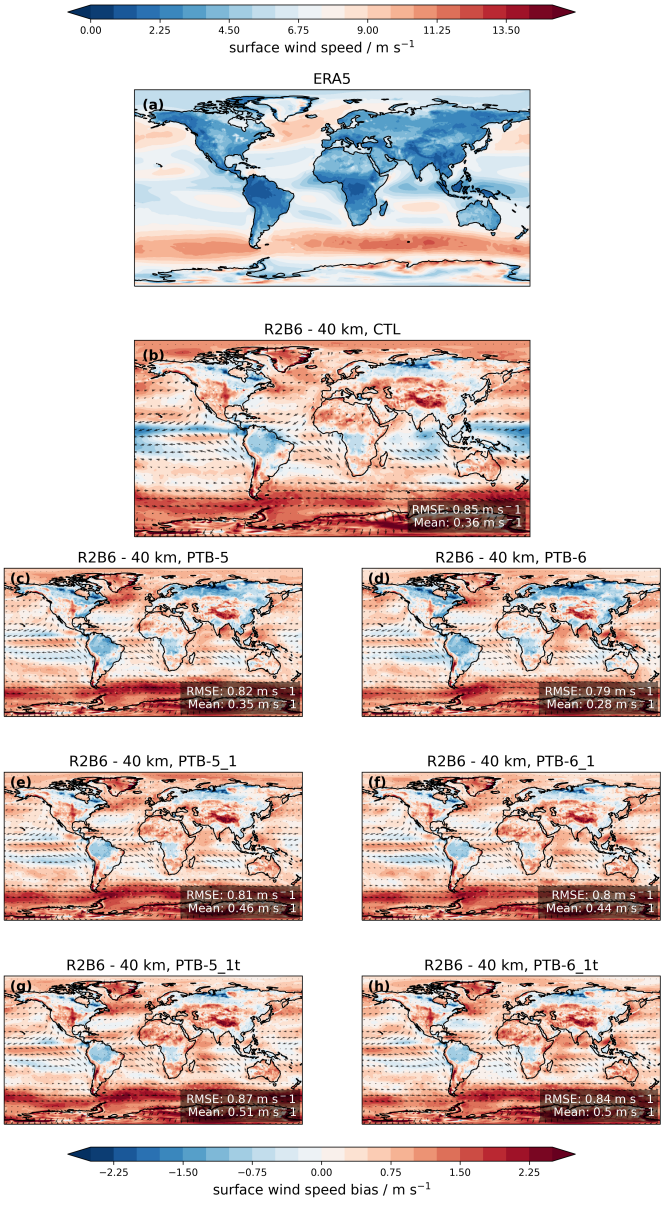

Figure 5. (a) ERA5 multi-year average near surface wind speeds for the years 2004-2010. (b-h) Two-year mean large-scale near-surface wind speed bias with respect to ERA5 for CTL and different settings of the near-surface wind speed limiter, U_{min}, in R2B6 (40 km) : PTB-5, PTB-5_1, PTB-5_1t, PTB-6, PTB-6_1 and PTB-6_1t. Arrows visualizing the near-surface wind speed for ERA5 are superimposed on the field change to visualize the general circulation (b-h). The root mean square error and mean error with respect to ERA5 are listed in the bottom right corner for the difference plots (b-h).

https://doi.org/10.5194/egusphere-2025-1212
Preprint. Discussion started: 25 March 2025

A comparison of the probability density function of monthly mean surface wind speeds in CTL, PTB-5, PTB-5_1, PTB-6 and PTB-6_1 with ERA5 in Fig. 6 over (a) the entire area between 10° S to 10° N, (b) sea-only and (c) land-only values summarizes how the changes in U_{min} feed back on the wind distribution (Fig. 6). Compared to ERA5, CTL exhibits a skew to smaller surface wind speeds which is visible in the wind speed distribution for all selected areas. This mainly reflects the weak Walker Circulation strength in the inner tropics. The skew to smaller near-surface wind speeds can be corrected via adjustment of U_{min} in the sea-only area, as seen by improvements in PTB-5, PTB-5_1, PTB-6 and PTB-6_1 (b). For the values over land (c), which are mainly in the velocity bins from 0 m s^{-1} to 2.5 m s^{-1}, the main velocity peak remains essentially unchanged in location across all ICON simulations. However, for the land corrected sensitivity tests PTB-5_1 and PTB-6_1 as well as CTL which also has a U_{min} of 1 m s^{-1}, an increase in the frequency of velocities nearer to 2.5 m s^{-1} wind speed is seen compared to PTB-5 and PTB-6. This feedback of U_{min} on the actual simulated velocity distribution over ocean is in accordance with the starting hypothesis stated above: It is most likely tied to the improved representation of the moisture distribution which wins out over the increases in the drag on the near surface winds. As the Warm Pool is now supplied with the required moisture to fuel the deep convection, the Walker circulation is strengthened, the free troposphere is warmed and the corresponding temperature anomaly is propagated through the entire tropics in accordance with the weak temperature gradient theory. Warming aloft increases the inversion over the East Pacific, which could potentially further increase the wind speeds by promoting low cloud formation in the East Pacific and feeding back on the Walker Circulation strength. As seen however in 5, the increased drag on the near-surface wind speeds will reduce near-surface wind speeds in higher latitudes - even within the tropics - as the feedback of the increased deep convection on the Walker Circulation and corresponding near-surface wind speed increase is confined to the inner tropics.

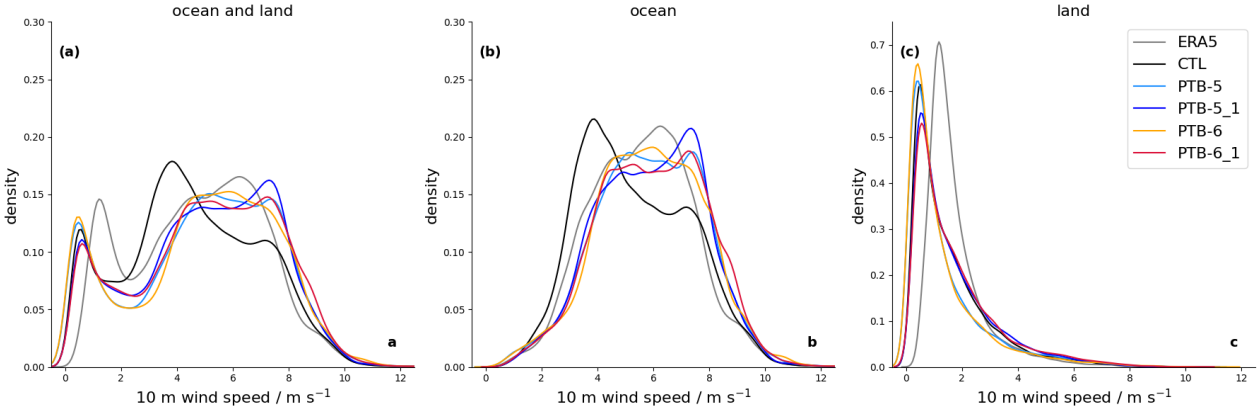

Figure 6. Normalized probability density functions for the zonally averaged monthly mean near-surface wind speed distributions between 10° S to 10° N in the experiments CTL, PTB-5, PTB-5_1, PTB-6 and PTB-6_1. A comparison with ERA5 data is given for (a) the entire region, (b) over sea only, and (c) over land only.

https://doi.org/10.5194/egusphere-2025-1212
Preprint. Discussion started: 25 March 2025

The changes in the spatial wind speed patterns (Fig. 5) have demonstrated that U_{min} has the potential to substantially impact the general atmospheric circulation. It increases the Walker Circulation strength but leads to a reduction of the Southern Hemispheric Trade Winds, which transport a substantial amount of moisture into the inner tropics. The change in U_{min} therefore comes at the risk of changing the weighting of the inner tropical versus outer and subtropical moisture sources. The analysis of the latent heat flux changes of CTL, PTB-5, PTB-5_1, PTB-6 and PTB-6_1 with respect to ERA5 can give some indication of potential changes in the moisture sources (cf. Fig. 7). We additionally show latent heat fluxes from the OAFlux data set which specifically focuses on surface fluxes and integrates satellite and buoy measurements as the latent heat flux is not assimilated in ERA5. In the bias plots a positive evaporation bias with too much moisture release to the atmosphere is visualized in blue, whereas an insufficient evaporation is visualized in red. It is apparent that the latent heat flux by ERA5 is larger than by OAFlux (Fig. 7 (a)-(d)). CTL shows too little latent heat flux in the region of the ITCZ in the Pacific as well as in the Indian Ocean with respect to ERA5 (Fig. 7 (c)). With respect to OAFlux (Fig. 7 (d)), which shows lower latent heat fluxes than ERA5 (Fig. 7 (b)), a general overestimation of latent heat fluxes is already present in CTL, with only a negligible underestimation near the Warm Pool and at the ITCZ. With the increase in U_{min} (Fig. 7(e),(f)), the low biases in the Warm Pool region are reverted to positive latent heat flux biases, leading to an excess latent heat flux in the tropical region, even compared to the already high values simulated by ERA5. In the Eastern Pacific, the negative evaporation bias in the northern ITCZ region is reduced. However, especially in the Central Pacific, a more pronounced positive bias develops as more moisture evaporates with the higher near surface wind speeds. This change occurs in a region where OAFlux and ERA5 show relative consistency. Additionally, negative evaporation biases emerges in the Trade Wind regions at the coasts of Middle- and South-America, indicating a reduction of the outer- and subtropical moisture source. All in all, there is a shift in the location of evaporation from the outer- and subtropics to the tropics in the perturbation experiments compared to CTL, leading to a reduction in spatial contrasts in evaporation biases. However, there is an increase in global-mean latent heat flux leading to too much evaporation overall.

https://doi.org/10.5194/egusphere-2025-1212
Preprint. Discussion started: 25 March 2025

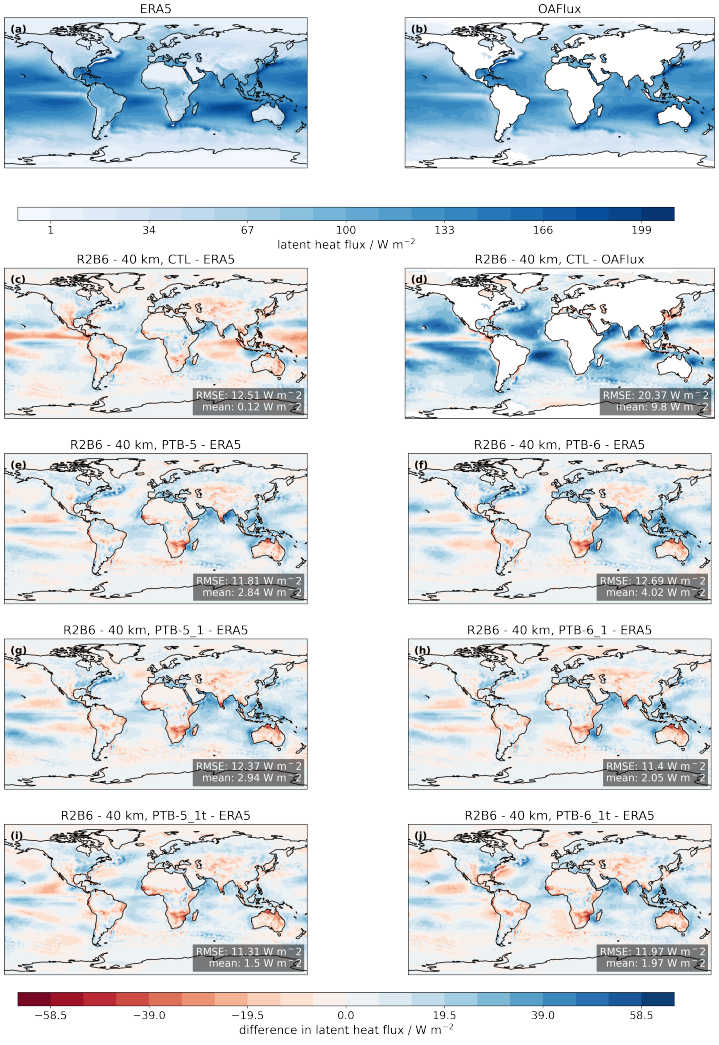

Figure 7. Latent heat flux in reanalysis and R2B6 simulations. (a) ERA5 multi-year average latent heat flux for the years 2004-2010. (b) OAFlux multi-year average latent heat flux for the years 2004-2010. (c) Two-year mean large-scale latent heat flux change of CTL with respect to ERA5 and OAFlux. (e-j) Two-year mean large-scale latent heat flux change with respect to ERA5 for CTL as well as the different settings of U_{min} in R2B6 (40 km) : PTB-5, PTB-5_1, PTB-5_1t, PTB-6, PTB-6_1 and PTB-6_1t. The root mean square error and mean error with respect to ERA5 are listed in the grey boxes of the graphs (c-j).

https://doi.org/10.5194/egusphere-2025-1212
Preprint. Discussion started: 25 March 2025

As we have seen far-reaching impacts on the general atmospheric circulations when U_{min} is increased, we investigate the impact of the altered U_{min} on other physical key parameters in Fig.8. The first parameter pair is the asymmetry index A_p and symmetry index E_p of the precipitation distribution. All sensitivity experiments show a positive A_p consistent with the observational references IMERG and GPCP indicating that the inter-hemispheric energy imbalance is captured correctly. E_p shows negative values, starting to increase only at a U_{min} of 4 m s^{-1}. This value, which reflects the large dry bias over the Warm Pool, indicates that the net energy input (NEI) to the atmosphere at the equator is most likely low biased. Since U_{min} preferentially effects evaporation in warm regions where evaporation is climatologically high and regions with low wind speeds, an increase in near-surface wind speed will have a more substantial effect in the inner-tropics (cf. Fig. 7), which would positively reflect in the E_p index, as is evident in the simulation scores.

The simulations scores also show how the global latent heat flux increases with increasing U_{min} which is also reflected in an increase in the near-surface specific humidity. A comparison of both values with the corresponding reference from ERA5 shows that whereas the bias in near-surface specific humidity decreases, the latent heat flux bias increases (cf. Fig. 7 and Fig. C1 for spatial maps). The high bias in the global latent heat flux in combination with the low bias in global near-surface specific humidity point towards an additional underlying problem for which U_{min} only combats the symptoms rather than the root cause.

Insight into the underlying problem can be inferred from examining the spatial maps of latent heat flux and near-surface specific humidity biases and their changes (Fig. 7 and Fig. C1). The increase in U_{min} leads to a reduction of latent heat flux RMSE as negative biases are reduced in the inner tropics, but it does this at the cost of an increase of the mean latent heat flux high bias as positive biases remain high in the subtropics, which in other words would say that the large bias in spatial patterns is reduced at the cost of a more uniform bias. This indicates that in total there is enough moisture available in the atmosphere through evaporation, but there are problems with the moisture distribution through the global circulation. U_{min} seems to compensate for three problems in the moisture transport. First, for a too strong transport out of the boundary layer in the 0-30 latitude band. Second, for a consequently too weak horizontal equatorward near-surface specific humidity transport within the Trades from the outer and tropics, the main source region of inner tropical moisture (Schneider et al., 2014). Third, for an insufficient upward transport of this moisture in the main deep convective regions by supplying a surplus in moisture. We will revisit this hypothesis in the overall interpretation of the coarse and high-resolution simulations in section 3.3.

The improvements of ITCZ bias and near-surface specific humidity comes at the cost of strong biases in the global year-mean net top-of-the-atmosphere (TOA) imbalance which drops by almost 4 W m^{-2} for a U_{min} of 5 m s^{-1} and 5 W m^{-2} respectively for a U_{min} of 6 m s^{-1} (Fig. 8). The main contribution to the changes in TOA imbalance arise from upward shortwave radiation which increases substantially as the cloud cover increases. Due to the specified-SST setup and the timeframe of the simulations, the increased bias in TOA imbalance can only have small effect on the surface temperature T_s arising from the sea ice and land only. Despite the negative TOA, T_s increases by around 1 K. This can be explained by the increase in free tropospheric moist

https://doi.org/10.5194/egusphere-2025-1212
Preprint. Discussion started: 25 March 2025

static energy, as both specific humidity values and atmospheric temperature increase while the lapse rate over land does not change substantially (Zhang and Boos, 2023). The increase in T_s is reflected in the increase in outgoing long wave radiation. The tuning simulations 5-1t and 6-1t (explained in Section 2.1.2) demonstrate that it is possible to readjust the radiative fluxes to expected values without strong deterioration in the improved precipitation distribution.

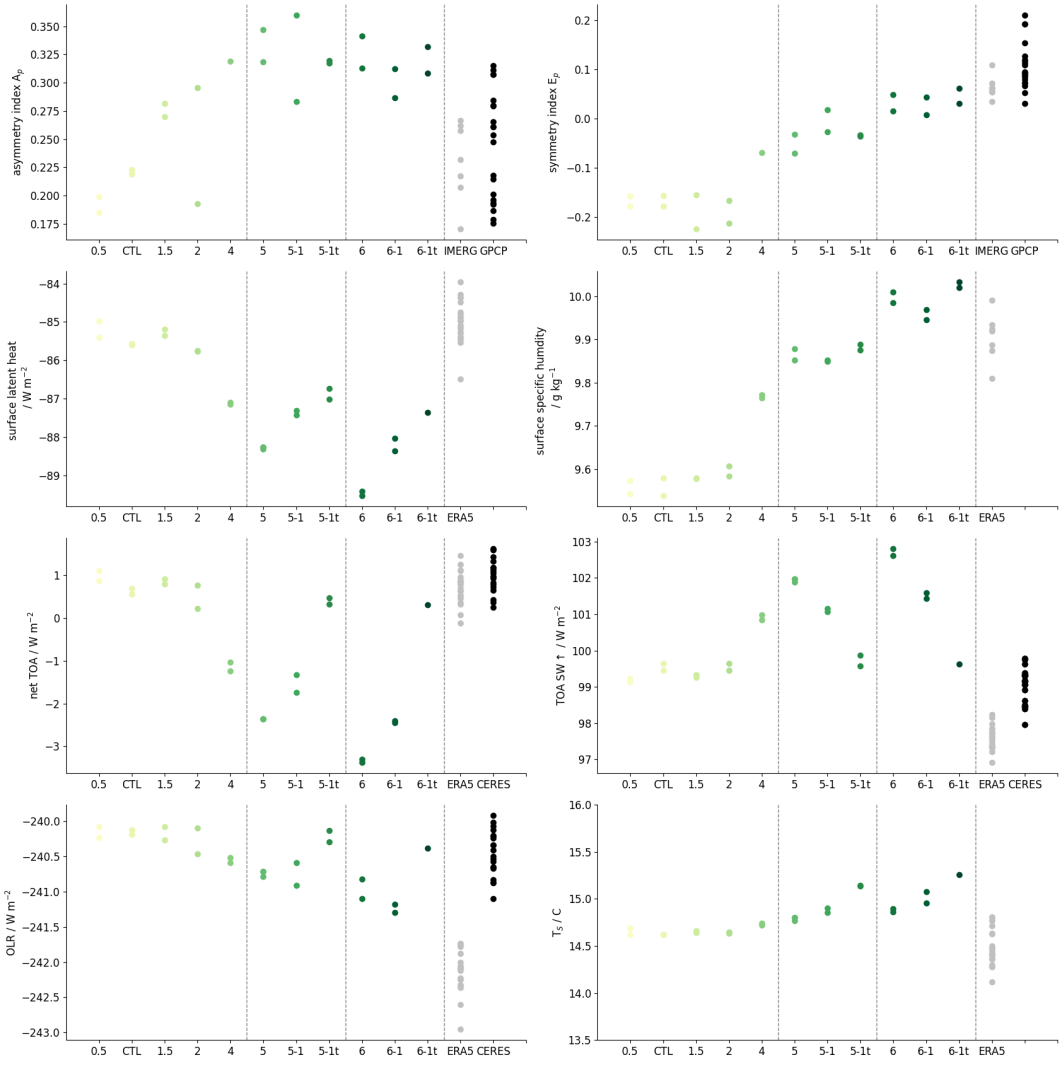

Figure 8. Tuning scores for all R2B6 (40 km) sensitivity experiments as a function of prescribed minimum surface wind speed. The values for a U_{min} of 1 are the CTL settings and where taken from the respective two years of the CTL simulation. Values for the asymmetric index A_p, symmetry index E_P as well as latent heat flux, near-surface specific humidity q_s, net top-of-the-atmosphere (TOA) imbalance, upwards radiative shortwave flux, outgoing long wave radiation (OLR) and global mean surface temperature T_S are shown. Each point depicts one global year average. For reference the corresponding values from IMERG, GPCP, ERA5 and CERES are depicted.

https://doi.org/10.5194/egusphere-2025-1212
Preprint. Discussion started: 25 March 2025

Within this section we have answered the first part of the second and a large portion of the third research question: The precipitation biases in coarse scale 40 km simulations can be addressed by increasing evaporation via an increase in U_{min} in the turbulence scheme. Mechanistically, the increase in U_{min} should lead to an increase in the drag on the surface winds. In the inner tropics however, the increase in U_{min} also counterbalances the dry bias in the Warm Pool region through its influence on evaporation. This fuels deep convection and leads to an acceleration of the Walker circulation transporting spurious moisture over the Eastern and Central Pacific into the main convective region. The increase in the Walker Circulation strength counterbalances the increases in drag on the near-surface wind speeds in the inner tropics, leading to an increase in near-surface wind speed over ocean. In the subtropics, which do not benefit from the increase Walker Circulation strength, the increased drag on the surface winds leads to a reduction in the Trade Wind strength. The improved representation of the ITCZ therefore comes at the cost of an replacement of higher latitude (sub)tropical moisture sources by an increase in the inner-tropical moisture source, a reduction in the Trade Wind strength and an increased global mean latent heat flux bias (cf. Fig.13).

3.3 Transferability to higher resolutions

After understanding the sensitivity to U_{min} changes in the coarser R2B6 setup, we proceed to answer the second part of research question 2 and test if the corresponding improvements also translate to the higher resolution, R2B9 (5 km). Due to computational constraints, we concentrate on seasonal rather than yearly averages in the precipitation feature, focusing on two MAM seasons, as it is the key season for the dITCZ bias (e.g., Si et al. (2021); Adam et al. (2018)). A comparison of the precipitation bias for the CTL, PTB5-1 and PTB5-1t simulations in R2B6 and R2B9 is shown in Fig. 9, demonstrating that biases are also reduced by U_{min} changes in the higher resolution simulations. Within the seasonal comparison, the R2B9 already shows a reduced RMSE compared to R2B6. It can therefore be expected that R2B9 is likely to outperform the coarser resolution simulations also in longer timeframe simulations, as was already the case in the CTL simulations (Fig. 1). Again, it is especially noticeable that the R2B9 does not exhibit the persistent dry bias over the islands over the Maritime continent. The positive precipitation bias appearing in the Indian Ocean with the U_{min} adjustments is not as prominent in higher resolution. Both resolutions show remaining precipitation biases in the Atlantic. However, while the ITCZ precipitation bias over the Atlantic is fused to a single precipitation band with Northward emphasis in R2B9, it is more diffuse in the R2B6 simulations with a more pronounced southern emphasis. The seasonal location of the ITCZ in MAM has a tendency towards the South (Berry and Reeder, 2014). In this regard the R2B6 Atlantic bias could improve the A_s index (cf. Fig. 12), whereas the R2B9 Atlantic bias deteriorates it. In contrast to the R2B6 simulations, the mean near-surface specific humidity bias is not fully neutralized in the R2B9 setup, although it is more than halved.

https://doi.org/10.5194/egusphere-2025-1212
Preprint. Discussion started: 25 March 2025

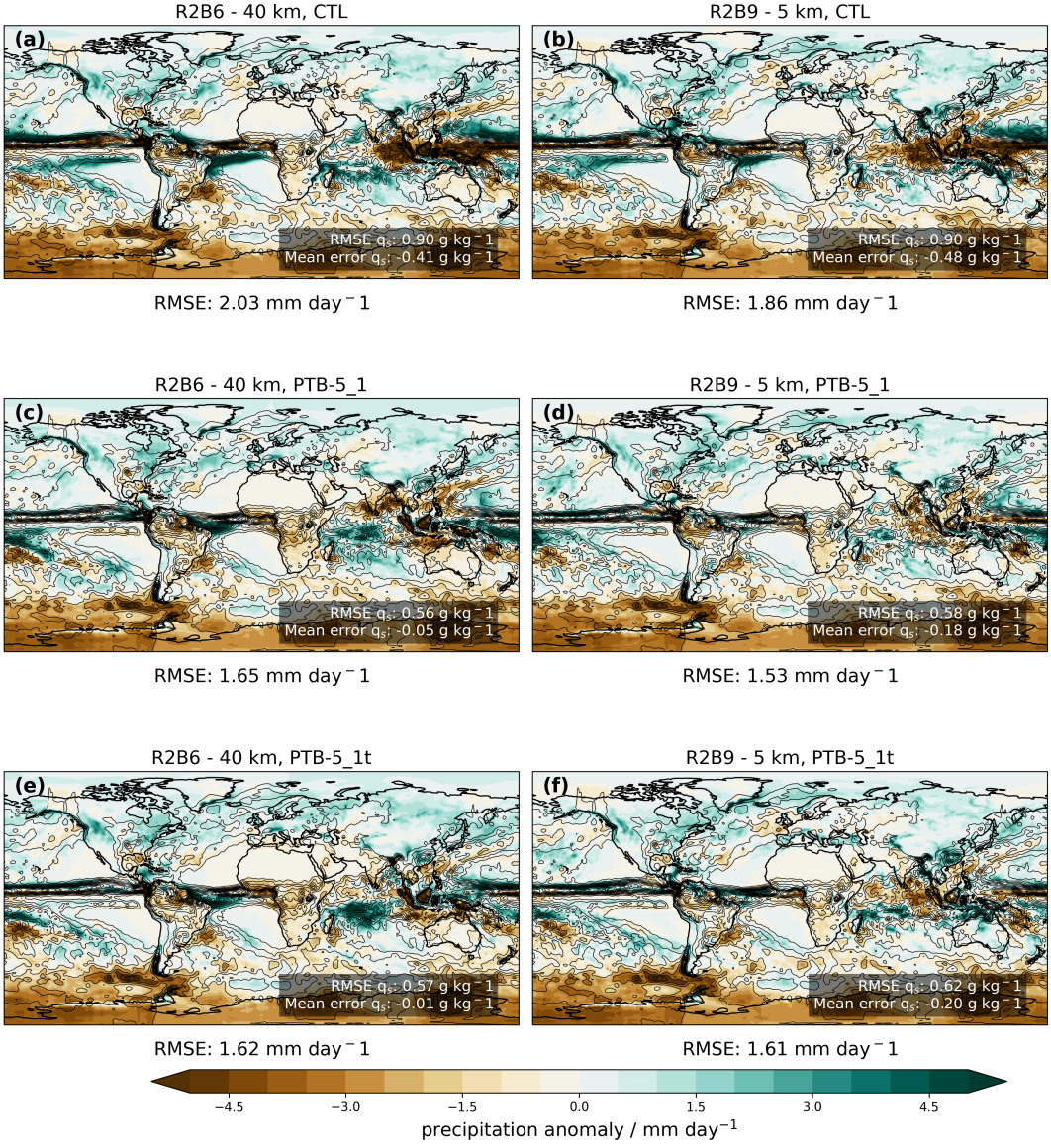

Figure 9. Large-scale precipitation bias with respect to IMERG in the MAM season: all CTL, PTB-5_1 and PTB-5_1t for R2B6 (40 km) and R2B9 (5 km). Contours show the IMERG MAM climatology. The corresponding global RMSE is stated beneath the panel for each sensitivity experiment. The global RMSE and mean error in near-surface specific humidity calculated with respect to values derived from ERA5 reanalysis is depicted in the inlays.

Figure 10 visualizes the changes in the bias of the zonal specific humidity distribution in MAM for R2B6 and R2B9 against ERA5, both for the untuned and tuned PTB-5_1 versions. In R2B6, the dry bias in the inner tropics reverses (from Subfig. (a) to (c) and (e) in Fig. 10), while the bias between 40 t o 20 °latitude above 1 to 2 km deteriorates. This again hints at the too efficient vertical transport out of the boundary layer into the free troposphere, most likely in regions of shallow convection,

https://doi.org/10.5194/egusphere-2025-1212
Preprint. Discussion started: 25 March 2025

and insufficient horizontal moisture transport starting at 30 latitude into the tropics. In R2B9-CTL, the near surface dry bias is far more pronounced than in R2B6-CTL, changing the baseline for the tuning. The increase in U_{min} reduces the dry bias and changes the sign of the inner-tropical dry bias up to 3 km, greatly reducing it in the levels above. At 20°N, the near surface dry bias improves without disappearing, whereas it almost disappears at 20°S. The reduced dry bias in the Southern Hemisphere leads to an increase of the moist bias in higher atmospheric levels whereas the situation in the Northern Hemisphere remains approximately unchanged. Overall, with increased U_{min} the specific humidity bias changes to positive everywhere in the lower resolution and biases are reduced in magnitude in the higher resolution. The remaining surface bias amounts to a percental bias of less than 3 percent resp. 15 percent of the background values in R2B6 and R2B9. Overall, despite the outlined differences in the resolutions, both R2B6 and R2B9 exhibit the same symptoms of a too strong vertical moisture transport from the boundary layer into the free troposphere between 40 t o 20 °latitude, which comes at the cost of reduced near-surface moisture transport into the tropics.

https://doi.org/10.5194/egusphere-2025-1212
Preprint. Discussion started: 25 March 2025

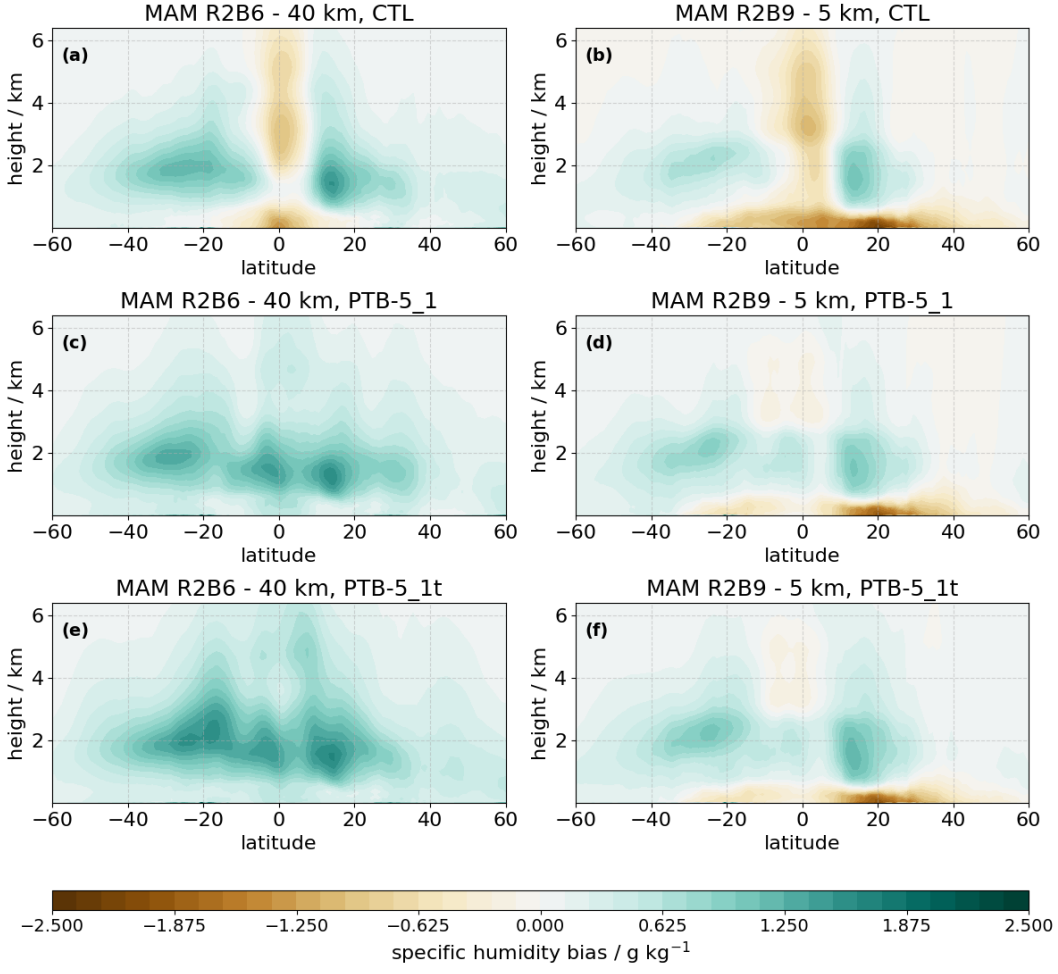

Figure 10. Atmospheric specific humidity bias for two MAM seasons with respect to ERA5 for R2B6-CTL, R2B6-PTB-5_1 and R2B6-PTB5-1t (40 km) as well as R2B9-CTL, R2B9-PTB-5_1 and R2B9-PTB5-1t (5 km) setups.

The increase in atmospheric specific humidity and deep convection in the inner tropics is also visible in the zonal mean temperature biases in Fig.11. The tropical free troposphere warms in both resolutions as the convection ties the temperature profile to a different base line moist adiabat with increased moisture supply. In R2B6 the bias is overcompensated resulting in a warm

https://doi.org/10.5194/egusphere-2025-1212
Preprint. Discussion started: 25 March 2025

bias, whereas the R2B9 resolution shows an overall improvement.

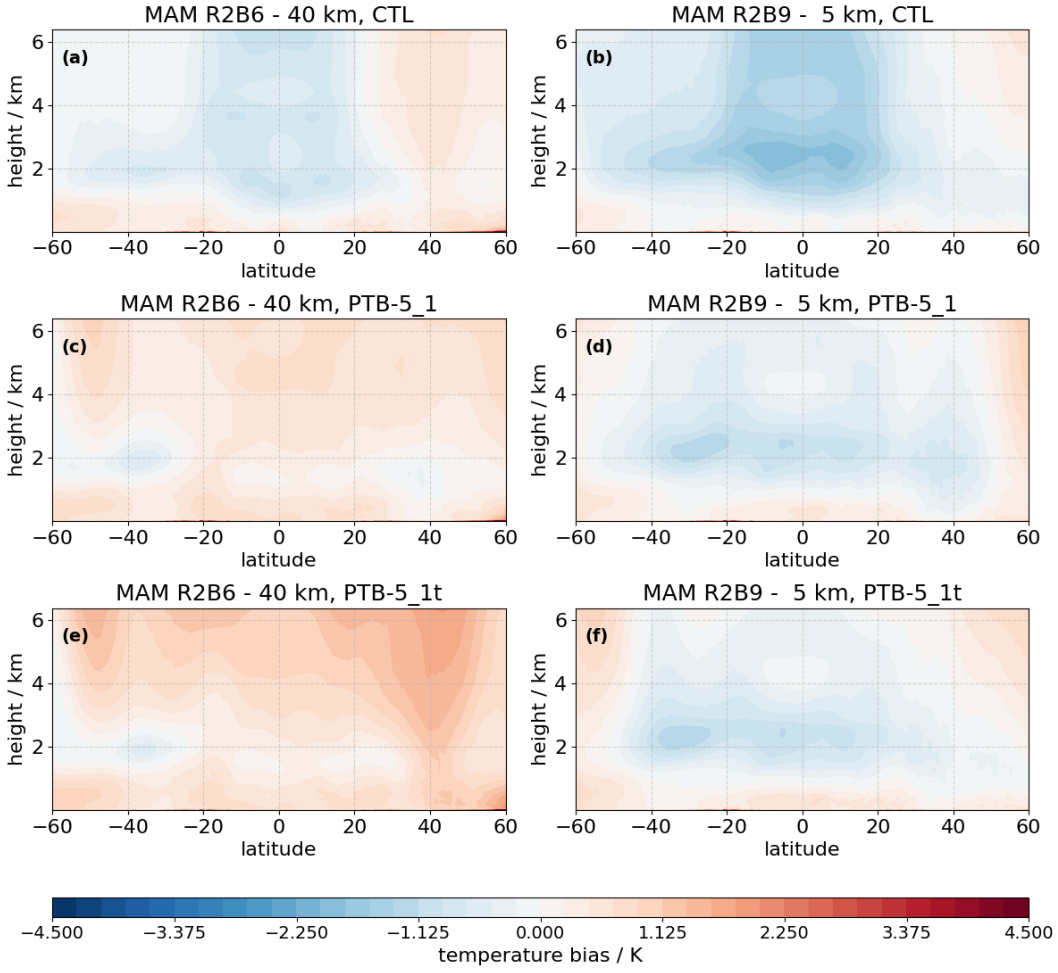

Figure 11. Zonal mean temperature bias for two MAM seasons with respect to ERA5 for CTL, PTB-5_1 and PTB-5_1t in R2B6 (40 km) as well R2B9 (5 km) setups.

https://doi.org/10.5194/egusphere-2025-1212
Preprint. Discussion started: 25 March 2025

The simulation scores are summarized in Fig.12, where the re-tuning was performed with the same parameter adaptations used in R2B6 (40 km) to test the transferability of the tuning to higher resolution. In almost all variables, R2B6 and R2B9 behave similarly, although it is also evident that the R2B9 simulations exhibit a greater spread (i.e., variability) than the coarser R2B6 counterpart for some variables. In A_s all simulations perform well compared to IMERG. The E_p score is already almost within observational constraints in the untuned version and improves for both resolutions with wind surface tuning. The improvement in near-surface specific humidity comes at the cost of an increased bias in latent heat flux, again indicating problems in the vertical and horizontal moisture transport. The top-of-the-atmosphere radiative imbalance shows increased variability in the R2B9 simulations. The main simulation from which the sensitivity experiments were branched off shows maximum jumps in year-mean TOA imbalance of 0.4 Wm^{-2} with no clear trend in the three simulated years, so there is no indication of a spin-up problem. Instead the resolved convective processes probably play a role in the increased variability, as they will show their signature in both the SW up (especially low clouds) and OLR (especially high clouds). The T_s is the only parameter in which the two resolutions show opposing trends with adjustment of the U_{min} and tuning: warming for R2B6 and cooling for R2B9. For both resolutions, the tuned versions are coming nearer to observational values however. As T_s is very closely related to orographic wave drag which again depends on the representation of the topography, resolution differences with otherwise identical tuning can be expected.

https://doi.org/10.5194/egusphere-2025-1212
Preprint. Discussion started: 25 March 2025

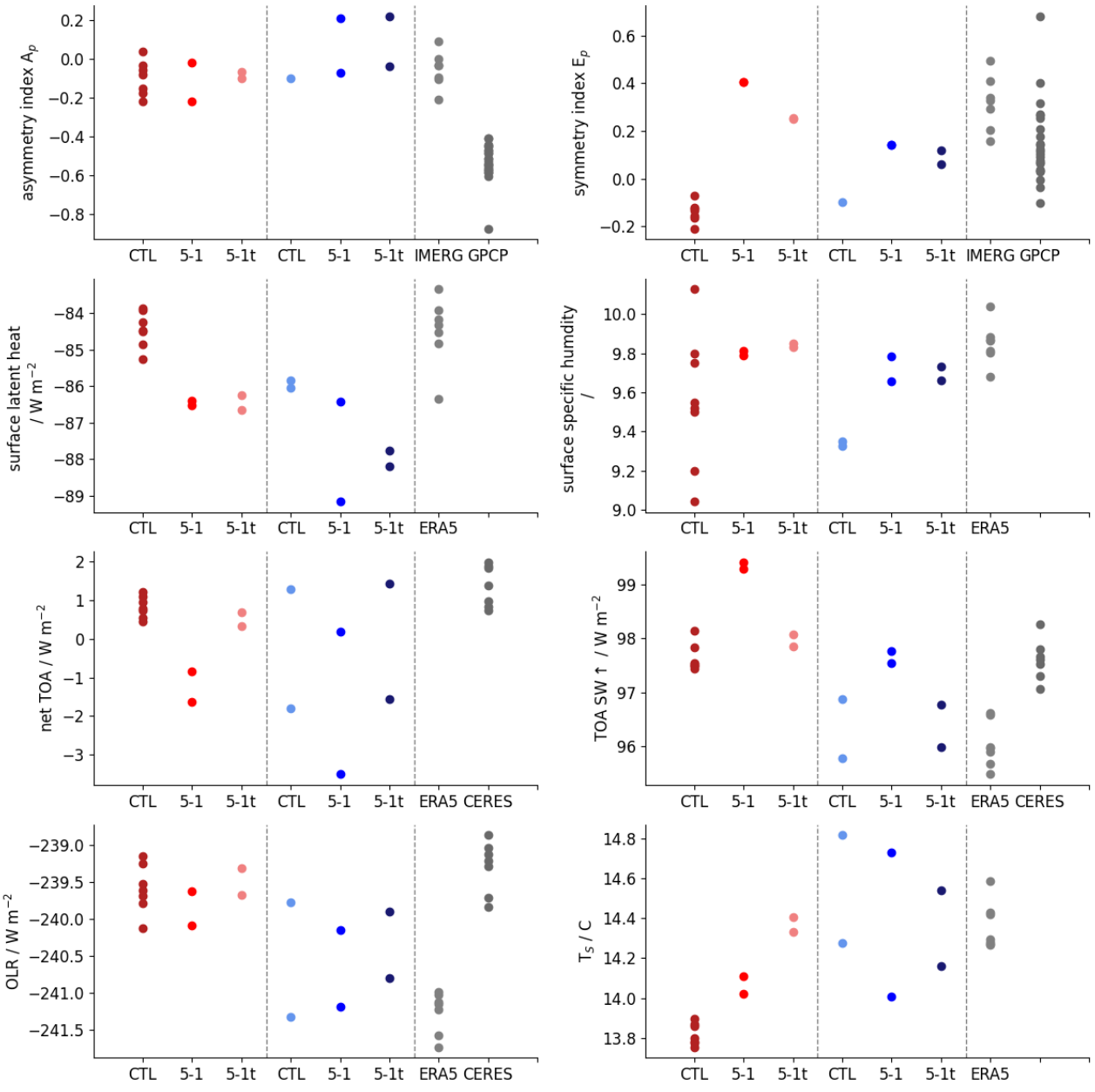

Figure 12. Tuning scores for two MAM seasons of the R2B6 (40 km) and R2B9 (5 km) CTL as well as their PTB-5_1 and PTB-5_1t sensitivity experiments. The R2B6 (40 km) scores are shown in different shades of red, the R2B9 (5 km) in different shades of blue. Values for the asymmetric index A_p, symmetry index E_P as well as latent heat flux, near-surface specific humidity q_s, net top-of-the-atmosphere (TOA) imbalance, upwards radiative shortwave flux, outgoing long wave radiation (OLR) and global mean surface temperature T_S are shown. Each point depicts a one season average. For reference the corresponding values from IMERG, GPCP, ERA5 and CERES are listed.

https://doi.org/10.5194/egusphere-2025-1212
Preprint. Discussion started: 25 March 2025

Summarizing the main findings in this section, we demonstrated the transferability both of U_{min} adjustment to counteract the development of the dITCZ as well as the R2B6 tuning to the R2B9 simulations. We showed that also humidity and temperature fields change in a similar fashion but different amplitude to U_{min} adjustments. In addition, we discussed the underlying mechanisms in more detail. Specifically, that the actual root cause of the dITCZ bias is not the dry bias in the Warm Pool, but an insufficient transport of moisture from within the 0-30 latitude band to the inner tropics (cf. Fig. **??**). Indications for this are found in Fig. 5, Fig. 7, Fig. 8 and Fig. 10.

4 Discussion and Conclusions

In our study, we compared the representation of the precipitation as simulated by ICON over a resolution hierarchy spanning from CMIP-resolution up to km-scale. Although some small-scale improvements, such as a better representation of precipitation over land with more pronounced orography were found, increased resolution and the discard of deep convective and non-orographic gravity wave parametrization could not resolve persistent large-scale precipitation biases. The large-scale precipitation biases found in our ICON resolution hierarchy are consistent with the dITCZ bias present through several CMIP generations (Tian et al., 2024). Additionally, we find a too-cold and too-moist free troposphere, which are especially pronounced in the midlatitudes, although the latter already emerge at around 20° latitude. These biases are symptoms of a general misrepresentation of the exchange of energy and moisture between the inner- and outer tropics (Fig. 13 (a), cf. Fig. 13 (b)).

To address the biases, we focused on the parameterizations that remain active at the km-scale, focusing on U_{min} in the turbulence scheme, which yielded promising results in the Sapphire configuration of the ICON model (Hohenegger et al., 2022; Segura et al., 2024). The usage of U_{min} in the bulk flux formula resolved some of the precipitation biases; however, we found a deterioration of precipitation over the land making a separate adjustment necessary. This was not seen in Segura et al. (2024) due to their focus on the dITCZ feature in the Warm Pool region. Furthermore, we showed that the wind surface tuning led to similar changes at the km-scale as in our lower-resolution simulations, indicating that tuning lessons learned at lower resolution can be applied to km-scale simulations. Our analysis also gives new insights into the mechanisms by which U_{min} acts: An increase in the wind speeds counterbalances the low biases in the near-surface specific humidity in the tropics, enhancing deep convective activity, which increases free tropospheric temperatures and the temperature inversion in subsidence regions.

However, further analysis also made some caveats with respect to changes in U_{min} evident. Although U_{min} improves the representation of the mean of the wind speed distribution in the innermost tropics, it introduces biases in its regional and temporal variability seen by the turbulence scheme. The increase in the mean state makes wind extremes to appear less pronounced as part of the low wind speed spectrum is cut off by U_{min}. This concern can be attenuated when considering that the "prescribed" bias in the velocity distribution is only seen by the turbulence scheme. Additionally, Back and Bretherton (2005) have found that the correlation between wind speed and precipitation mainly is not related to mesoscale gustiness but triggered by increases in the mean surface fluxes.

Focusing on these very surface fluxes, it is known that the bulk flux formulation can lead to biased results compared to observations both in very low and very high wind regimes, producing a high bias in latent heat release(Hsu et al., 2022). This behavior

https://doi.org/10.5194/egusphere-2025-1212
Preprint. Discussion started: 25 March 2025

is also present in ICON. The uniform increase in U_{min} increases the latent heat flux bias globally, showing only improvements in the originally low-biased Warm Pool region. The increase of latent heat release in the Warm Pool region corrects for the lack in net energy input in the inner-tropical region which is implied by the E_p index. Given the negative impact on the biases in latent heat fluxes, we suggest that a wind speed limiter that accounts for regional differences in wind speed distributions would be a superior solution.

The fact that the model can not replicate the observed near-surface wind distribution hints at more overarching problems in the global near-surface moisture advection. The increase in U_{min} speed acts to address the too weak Walker Circulation but does not address the lack of moisture transport from the higher (sub)tropical latitudes starting at 30 °latitude, which is likely the origin of the tropical dry bias (Fig. 13 (c)). If this understanding is correct, the additional supply of near-surface moisture is drawn from the wrong location, i.e. the inner tropics instead of the higher latitude (sub)tropics. The study by Lang et al. (2023) who performed trajectory analysis for humidity parcels supports this hypothesis. They could demonstrate that tropical moisture biases are greatly influenced by insufficient transport from the higher latitude (sub)tropics. In addition, they described the tendency of the TTE turbulence scheme used in this ICON configuration to act similarly to a convection scheme, also in higher atmospheric layers. Huusko et al. (2025) in turn demonstrate that there are no significant changes in the turbulence boundary layer schemes with increasing resolution. Their and our findings combined would explain the positive moisture bias in the higher layers of the subtropical atmosphere - they are caused by the tendency of the turbulence scheme to transport moisture upwards out of the boundary layer like a convective scheme. Another source of the bias might also be the shallow convection; however, as the same bias was also encountered in the ICON sapphire configuration without the shallow convection, a bias in the used turbulence schemes or in the dynamical core is more likely.

In summary the main findings of this work are:

1. Similar large-scale precipitation biases persist throughout the ICON resolution hierarchy up to km-scale resolution, although improvements in orographically prominent regions appear with increasing resolution.

2. Precipitation biases can be resolved by adapting undiscardable parametrizations but only yield an overall improvement of the precipitation fields if ocean and land are treated separately. The direction of regional changes hold over various resolutions. The main driving mechanism is a strengthening of the Walker Circulation by increasing the supply of available moisture for the deep convective regions.

3. There are strong indications that this fix is not addressing the underlying core problem. A uniform wind threshold does not account for different regional circulation regimes and will lead to too high evaporation values in regions with low wind speed variations. Especially noticeable is also that the global latent heat flux and the 40 to 20 °latitude free tropospheric moisture bias are increased in the retuned simulations. This hints that there are problems with the source regions and transport of atmospheric moisture. There is some indication that the replacement of subtropical moisture by moisture originating from the inner tropics and the increase in drag on the near-surface wind speeds leads to a slow

https://doi.org/10.5194/egusphere-2025-1212
Preprint. Discussion started: 25 March 2025

down of the Trades winds which indicates that the adjustment might compromise the representation of extra-tropical to tropical teleconnections.

4. Results indicate a two-fold faulty representation of the moisture transport (including by parametrizations) in ICON, and potentially in the many other models with a dITCZ bias:

   - In the subtropics, the vertical moisture transport out of the boundary layer is too strong, leaving less moisture to be transported horizontally within the Trades into the tropics.
   - In the tropics, the lack of moisture reduces deep convective activity, which in turn reduces temperature inversions and slows down the Walker Circulation. The reduced zonally anomalous circulations favors the development of a second ITCZ branch as moisture is not transported into the core regions for deep convection.

The differences in moisture and energy export found in the observations, the world simulated in the CTL ICON and the ICON with wind speed adaptations are depicted in Fig.13.

The results of this study suggest that a two-fold climate modeling strategy would be greatly beneficial for the community: On the one side the advancement of high-resolution simulations by larger institutions with vast computational resources. On the other side the further development of necessary parametrizations and coarse-scale models in close collaboration with theoreticians. The persistence of large-scale biases found in our ICON resolution hierarchy shows the potential of learning both from high- and low-resolutions. This approach was also demonstrated in the tuning of the precipitation biases in the NICAM model which specifically addressed and learned from resolution independent biases (Takasuka et al., 2024). In the long term, scale-aware parametrizations, potentially with a seamless transition between convective and sub-grid scale turbulent processes within one unified scheme (i.e. Tan et al. (2018)), might build a bridge between the high- and low-resolution modeling strategies.

https://doi.org/10.5194/egusphere-2025-1212
Preprint. Discussion started: 25 March 2025

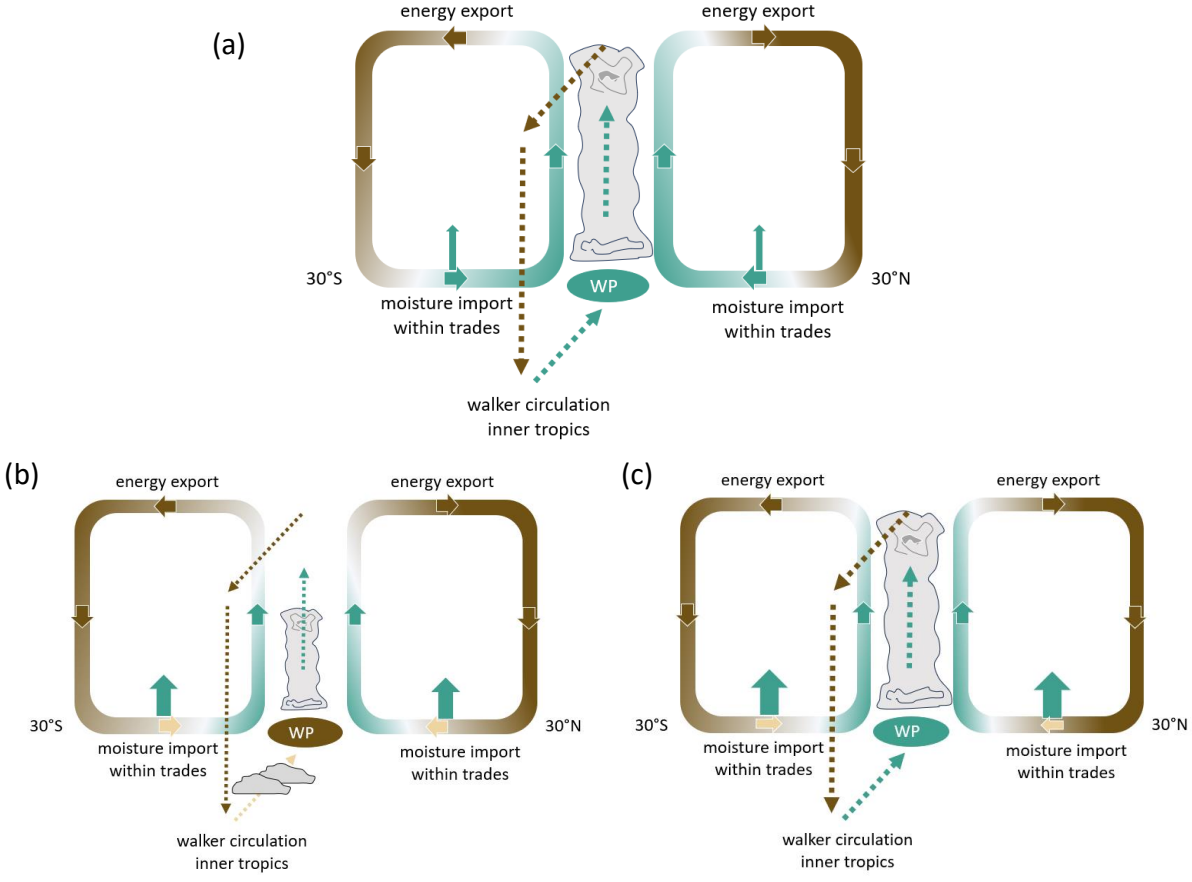

Figure 13. Conceptual depiction of the main zonal and meridional circulations exchanging moisture and energy between the subtropics and the tropics as a) observed, b) in conventional ICON simulations, and c) in U_{min} adjusted ICON simulations. Observations show that the moisture within the innermost tropics originates from evaporation in tropical and subtropical areas. The moisture is imported into the innermost tropics by the Trade Winds, with small losses to the free troposphere. In the innermost tropics it is then transported to the main convective regions, i.e., the Warm Pool (WP) within the zonally anomalous Walker circulation. Energy is exported to the subtropics within the outward branches of the Hadley circulation. In conventional ICON simulations (b), a large portion of moisture is lost due to too much vertical transport of moisture from the boundary layer to the free troposphere between 0°and 30°latitude. This leads to a moisture deficit in the tropics, specifically over the WP, reducing deep convection, slowing down the Walker Circulation and leading to spurious additional convective centers over the Eastern Pacific as too little moisture is transported to the WP within the boundary layer. In the wind speed corrected ICON world (c) increased surface wind speed lead to an additional moisture source in the tropics which resolves the dry bias over the WP. However, the adjustments increase the overexpressed free tropospheric moisture bias between 0°to 30°, reduce the Trade Wind strength, lead to a too strong Walker Circulation and most importantly change the balance between innermost-tropical to (sub)-tropical contribution to the tropical moisture content. Green colors indicate high moisture content. Brown colors low moisture content.

https://doi.org/10.5194/egusphere-2025-1212
Preprint. Discussion started: 25 March 2025

Code and data availability. The ICON code was released in January 2024 under https://www.icon-model.org/news/news_open_source_release. The ICON XPP code release and source scripts are publicly available and published by Müller et al. (2024). Model data and final postprocessing scripts needed to replicate the work presented in this paper will made available upon publication in a zenodo archive. The reanalysis data set ERA5 is available via the climate data store (https://cds.climate.copernicus.eu/). IMERG is provided by NASA under https://gpm.nasa.gov/data/directory. GPCP data sets are maintained by NOAA under https://psl.noaa.gov/data/gridded/data.gpcp.html. CERES data can be obtained from NASA under https://ceres.larc.nasa.gov/data/. OAFlux data is maintained by NCAR under https://climatedataguide.ucar.edu/climate-data/oaflux-objectively-analyzed-air-sea-fluxes-global-oceans. For postprocessing and data analysis python and CDO were used, the latter of which can be downloaded under https://code.mpimet.mpg.de/projects/cdo.

Appendix A

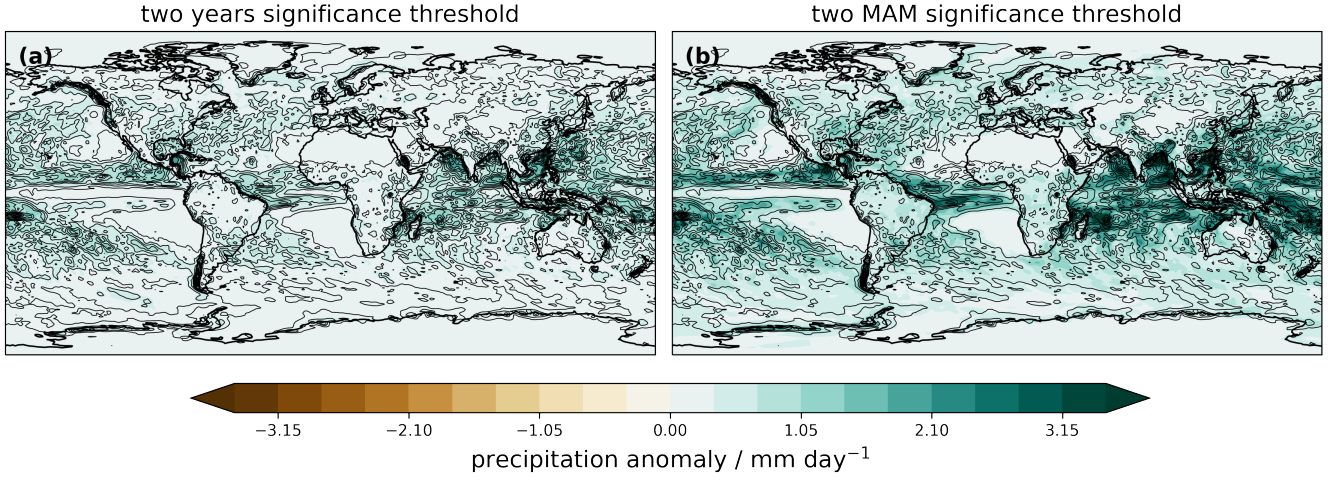

Figure A1. Significance threshold for a two sided z-test at α=0.1 based on the entire R2B6-CTL simulation. Values for a sample of two-years and two MAM seasons are shown. Autocorrelation is small for precipitation and can be neglected.

https://doi.org/10.5194/egusphere-2025-1212
Preprint. Discussion started: 25 March 2025

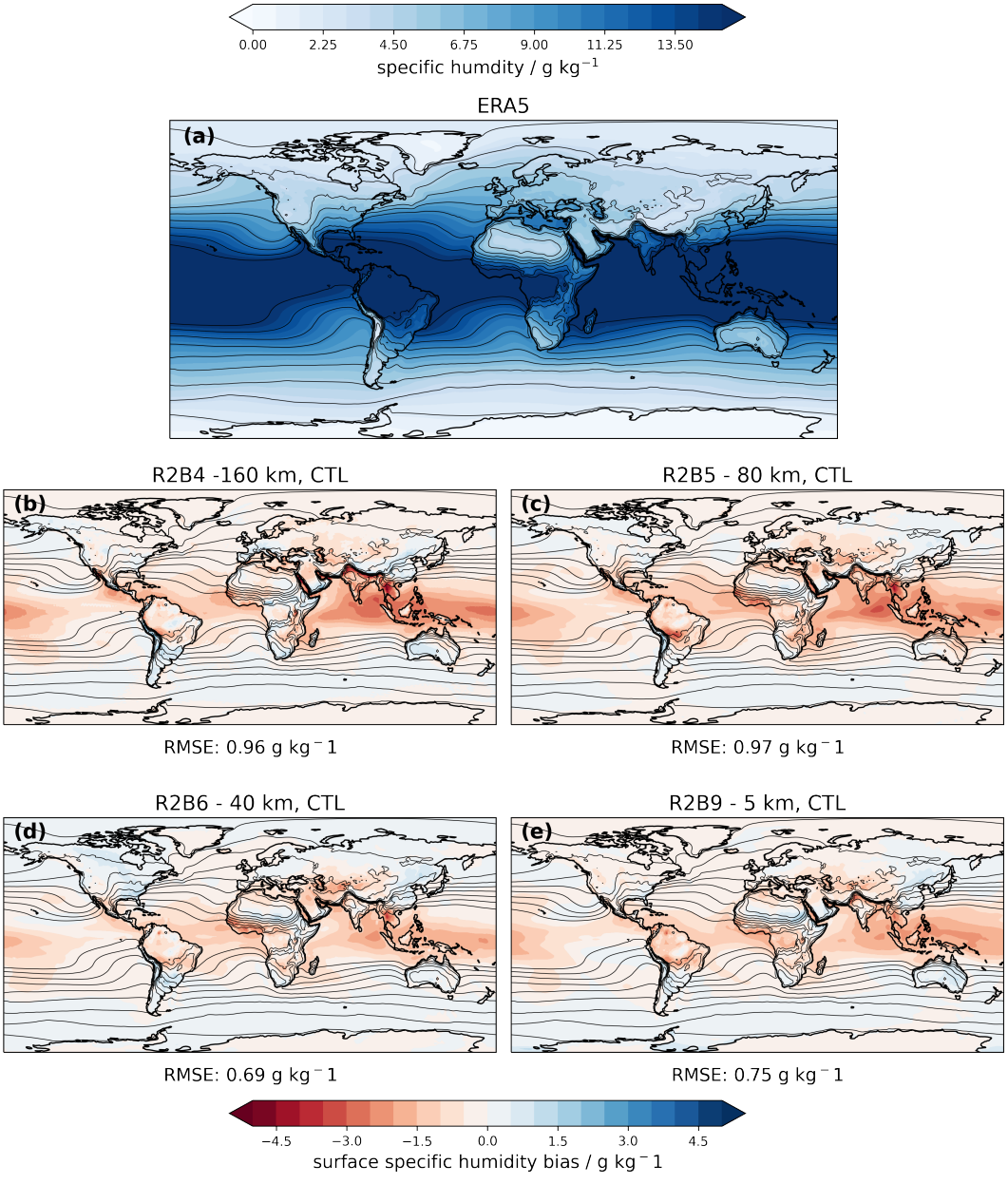

Figure B1. Two-year mean large-scale surface specific humidity bias with respect to ERA5 (2004-2010) over the resolution hierarchy. Global mean root mean square errors are shown below the plots.

https://doi.org/10.5194/egusphere-2025-1212
Preprint. Discussion started: 25 March 2025

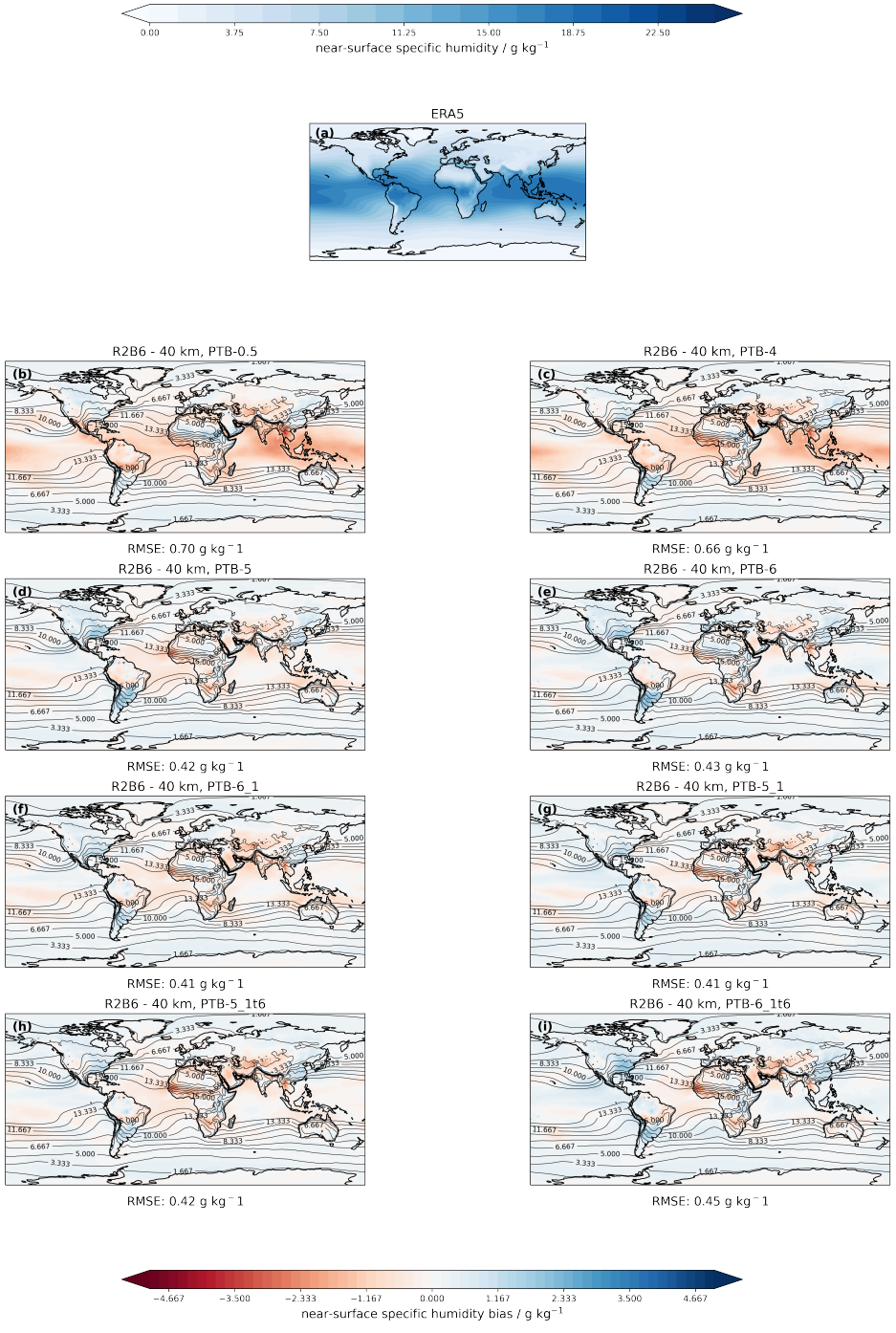

Figure C1. Two-year mean large-scale surface humdity bias with respect to ERA5 (2004-2010) for different settings of the surface wind in R2B6 (40 km): : PTB-0.5, PTB-4, PTB-5, PTB-5_1, PTB-5_1t, PTB-6, PTB-6_1 and PTB-6_1t. Contours show the ERA5 climatology. The corresponding global RMSE is stated beneath the panel for each sensitivity experiment.

https://doi.org/10.5194/egusphere-2025-1212
Preprint. Discussion started: 25 March 2025

Author contributions. CAK had the idea for the study, conceptualized it, acquired computational resources, performed the analysis and wrote the paper manuscript. Model simulations and tuning were done by UN in R2B4, by AS in R2B5 and CAK in R2B6 and R2B9. RJW provided input on many details of the analysis. LK advised on technical aspects on the model setup and provided the necessary input data. All authors contributed to the interpretation of the results and revised the paper manuscript.

Competing interests. The authors declare that they have no conflict of interest.

Acknowledgements. This research has been supported by the ETH Postdoctoral Fellowship Program (CAK), DWD's "Innovation Programme for Applied Researches and Developments" IAFE ICON-Seamless VH 4.7 (AS), the Swiss National Science Foundation Award PCEFP2 203376 (RJW) and the research unit FOR 2820 VolImpact (Grant 398006378) funded by the German Research Foundation (DFG) within the project VOLARC (UN). The authors specifically thank the ICON Seamless/ICON XPP Friends-circle and the XPP Precipitation task force for invaluable collaboration and support throughout the project year. This work greatly benefited from inspiring discussions with our colleagues Kristina Fröhlich, Karel Castro-Morales, Maike Ahlgrimm and Trang van Pham. It would not have been possible to run the ICON XPP code on GPU without Roland Wirth, who fixed some remaining GPU porting bugs. We thank Doris Folini for discussion with the authors. Computing and data storage resources for the R2B6 and R2B9 simulations, were provided by the Swiss National Supercomputing Center (CSCS) in Lugano via the project: s1283 and lp67 as well as the early-testers access to the vCluster Todi on the new Alps infrastructure. William Sawyer, Christoph Müller as well as the technical staff at CSCS have been very supportive of the ICON community when transitioning to the new Alps computing infrastructure. For the R2B5 simulations we thank the German Weather Services for providing computation resources on their system rts, for the R2B4 simulations, we thank the Deutsches Klima Rechenzentrum (DKRZ) for providing resources granted by its Scientific Steering Committee (WLA) under project ID bm0550.

https://doi.org/10.5194/egusphere-2025-1212
Preprint. Discussion started: 25 March 2025

References

Adam, O., Schneider, T., Brient, F., and Bischoff, T.: Relation of the double-ITCZ bias to the atmospheric energy budget in climate models, Geophysical Research Letters, 43, 7670–7677, https://doi.org/10.1002/2016GL069465, 2016.

Adam, O., Schneider, T., and Brient, F.: Regional and seasonal variations of the double-ITCZ bias in CMIP5 models, Climate Dynamics, 51, 101–117, https://doi.org/10.1007/s00382-017-3909-1, 2018.

Arakawa, A.: The Cumulus Parameterization Problem: Past, Present, and Future, Journal of Climate, 17, 2493–2525, 2004.

Back, L. E. and Bretherton, C. S.: The Relationship between Wind Speed and Precipitation in the Pacific ITCZ, Journal of Climate, 18, 4317–4328, https://doi.org/10.1175/JCLI3519.1, 2005.

Bechtold, P., Köhler, M., Jung, T., Doblas-Reyes, F., Leutbecher, M., Rodwell, M. J., Vitart, F., and Balsamo, G.: Advances in simulating atmospheric variability with the ECMWF model: From synoptic to decadal time-scales, Quarterly Journal of the Royal Meteorological Society, 134, 1337–1351, https://doi.org/https://doi.org/10.1002/qj.289, _eprint: https://rmets.onlinelibrary.wiley.com/doi/pdf/10.1002/qj.289, 2008.

Berry, G. and Reeder, M. J.: Objective Identification of the Intertropical Convergence Zone: Climatology and Trends from the ERA-Interim, Journal of Climate, 27, 1894–1909, https://doi.org/10.1175/JCLI-D-13-00339.1, 2014.

Bischoff, T. and Schneider, T.: Energetic Constraints on the Position of the Intertropical Convergence Zone, Journal of Climate, 27, 4937–4951, https://doi.org/10.1175/JCLI-D-13-00650.1, 2014.

C3S: ERA5 hourly data on single levels from 1940 to present, https://doi.org/10.24381/CDS.ADBB2D47, 2018.

Doelling, D. R., Loeb, N. G., Keyes, D. F., Nordeen, M. L., Morstad, D., Nguyen, C., Wielicki, B. A., Young, D. F., and Sun, M.: Geostationary Enhanced Temporal Interpolation for CERES Flux Products, Journal of Atmospheric and Oceanic Technology, 30, 1072–1090, https://doi.org/10.1175/JTECH-D-12-00136.1, 2013.

Doelling, D. R., Sun, M., Nguyen, L. T., Nordeen, M. L., Haney, C. O., Keyes, D. F., and Mlynczak, P. E.: Advances in Geostationary-Derived Longwave Fluxes for the CERES Synoptic (SYN1deg) Product, Journal of Atmospheric and Oceanic Technology, 33, 503–521, https://doi.org/10.1175/JTECH-D-15-0147.1, 2016.

Dong, Y., Armour, K. C., Battisti, D. S., and Blanchard-Wrigglesworth, E.: Two-Way Teleconnections between the Southern Ocean and the Tropical Pacific via a Dynamic Feedback, Journal of Climate, 35, 6267–6282, https://doi.org/10.1175/JCLI-D-22-0080.1, 2022.

Durack, P. J. and Taylor, K. E.: PCMDI AMIP SST and sea-ice boundary conditions version 1.1.4, https://doi.org/10.22033/ESGF/INPUT4MIPS.2204, 2018.

Fairall, C. W., Bradley, E. F., Hare, J. E., Grachev, A. A., and Edson, J. B.: Bulk Parameterization of Air–Sea Fluxes: Updates and Verification for the COARE Algorithm, Journal of Climate, 16, 571–591, https://doi.org/10.1175/1520-0442(2003)016<0571:BPOASF>2.0.CO;2, 2003.

Früh, B., Potthast, R., Müller, W., Korn, P., Brienen, S., Fröhlich, K., Helmert, J., Köhler, M., Lorenz, S., Pham, T. V., Pohlmann, H., Schlemmer, L., Schnur, R., Schulz, J.-P., Sgoff, C., Vogel, B., Wirth, R., and Zängl, G.: ICON-Seamless, the development of a novel Earth System Model based on ICON for time scales from weather to climate, https://doi.org/10.5194/ems2022-292, 2022.

Halpern, D. and Hung, C.: Satellite observations of the southeast Pacific intertropical convergence zone during 1993–1998, Journal of Geophysical Research: Atmospheres, 106, 28 107–28 112, https://doi.org/10.1029/2000JD000056, 2001.

Ham, Y.-G. and Kug, J.-S.: Effects of Pacific Intertropical Convergence Zone precipitation bias on ENSO phase transition, Environmental Research Letters, 9, 064 008, https://doi.org/10.1088/1748-9326/9/6/064008, 2014.

https://doi.org/10.5194/egusphere-2025-1212
Preprint. Discussion started: 25 March 2025

Hardiman, S. C., Boutle, I. A., Bushell, A. C., Butchart, N., Cullen, M. J. P., Field, P. R., Furtado, K., Manners, J. C., Milton, S. F., Morcrette, C., O'Connor, F. M., Shipway, B. J., Smith, C., Walters, D. N., Willett, M. R., Williams, K. D., Wood, N., Abraham, N. L., Keeble, J., Maycock, A. C., Thuburn, J., and Woodhouse, M. T.: Processes Controlling Tropical Tropopause Temperature and Stratospheric Water Vapor in Climate Models, Journal of Climate, 28, 6516 – 6535, https://doi.org/10.1175/JCLI-D-15-0075.1, 2015.

Held, I. M. and Hoskins, B. J.: Large-Scale Eddies and the General Circulation of the Troposphere, in: Advances in Geophysics, vol. 28, pp. 3–31, Elsevier, ISBN 978-0-12-018828-4, https://doi.org/10.1016/S0065-2687(08)60218-6, 1985.

Hersbach, H., Bell, B., Berrisford, P., Hirahara, S., Horányi, A., Muñoz-Sabater, J., Nicolas, J., Peubey, C., Radu, R., Schepers, D., Simmons, A., Soci, C., Abdalla, S., Abellan, X., Balsamo, G., Bechtold, P., Biavati, G., Bidlot, J., Bonavita, M., De Chiara, G., Dahlgren, P., Dee, D., Diamantakis, M., Dragani, R., Flemming, J., Forbes, R., Fuentes, M., Geer, A., Haimberger, L., Healy, S. B., Hogan, R., Hólm, E., Janisková, M., Keeley, S., Laloyaux, P., Lopez, P., Lupu, C., Radnoti, G., de Rosnay, P., Rozum, I., Vamborg, F., Villaume, S., and Thépaut, J.-N.: Fifth generation of ECMWF atmospheric reanalyses of the global climate. Complete ERA5 from 1940: Fifth generation of ECMWF atmospheric reanalyses of the global climate., https://doi.org/10.24381/cds.143582cf, 2017.

Hogan, R. J. and Bozzo, A.: A Flexible and Efficient Radiation Scheme for the ECMWF Model, Journal of Advances in Modeling Earth Systems, 10, 1990–2008, https://doi.org/https://doi.org/10.1029/2018MS001364, _eprint: https://agupubs.onlinelibrary.wiley.com/doi/pdf/10.1029/2018MS001364, 2018.

Hohenegger, C., Korn, P., Linardakis, L., Redler, R., Schnur, R., Adamidis, P., Bao, J., Bastin, S., Behravesh, M., Bergemann, M., Biercamp, J., Bockelmann, H., Brokopf, R., Brüggemann, N., Casaroli, L., Chegini, F., Datseris, G., Esch, M., George, G., Giorgetta, M., Gutjahr, O., Haak, H., Hanke, M., Ilyina, T., Jahns, T., Jungclaus, J., Kern, M., Klocke, D., Kluft, L., Kölling, T., Kornblueh, L., Kosukhin, S., Kroll, C., Lee, J., Mauritsen, T., Mehlmann, C., Mieslinger, T., Naumann, A. K., Paccini, L., Peinado, A., Praturi, D. S., Putrasahan, D., Rast, S., Riddick, T., Roeber, N., Schmidt, H., Schulzweida, U., Schütte, F., Segura, H., Shevchenko, R., Singh, V., Specht, M., Stephan, C. C., von Storch, J.-S., Vogel, R., Wengel, C., Winkler, M., Ziemen, F., Marotzke, J., and Stevens, B.: ICON-Sapphire: simulating the components of the Earth System and their interactions at kilometer and subkilometer scales, Geoscientific Model Development Discussions, 2022, 1–42, https://doi.org/10.5194/gmd-2022-171, 2022.

Holton, J. R.: An Introduction to Dynamic Meteorology, Academic Press, Amsterdam, Boston, 4th edition edn., 2004.

Hourdin, F., Mauritsen, T., Gettelman, A., Golaz, J.-C., Balaji, V., Duan, Q., Folini, D., Ji, D., Klocke, D., Qian, Y., Rauser, F., Rio, C., Tomassini, L., Watanabe, M., and Williamson, D.: The Art and Science of Climate Model Tuning, Bulletin of the American Meteorological Society, 98, 589–602, https://doi.org/10.1175/BAMS-D-15-00135.1, 2017.

Hsu, C., DeMott, C. A., Branson, M. D., Reeves Eyre, J., and Zeng, X.: Ocean Surface Flux Algorithm Effects on Tropical Indo-Pacific Intraseasonal Precipitation, Geophysical Research Letters, 49, e2021GL096 968, https://doi.org/10.1029/2021GL096968, 2022.

Hu, Z., Lamraoui, F., and Kuang, Z.: Influence of Upper-Troposphere Stratification and Cloud–Radiation Interaction on Convective Overshoots in the Tropical Tropopause Layer, Journal of the Atmospheric Sciences, 78, 2493 – 2509, https://doi.org/10.1175/JAS-D-20-0241.1, 2021.

Huffman, G. J.: GPCP Precipitation Level 3 Monthly 0.5-Degree V3.2, https://doi.org/10.5067/MEASURES/GPCP/DATA304, 2021.

Huffman, G. J., Bolvin, D. T., Nelkin, E. J., and Stocker, J. T.: V06 IMERG Release Notes, https://gpm.nasa.gov/sites/default/files/2020-10/IMERG_V06_release_notes_201006_0.pdf, 2010.

Huusko, L., Þórarinsson, P. , Pyykkö, J., and Svensson, G.: Resolution dependence of the turbulent atmospheric boundary layer in global storm-resolving climate simulations, Quarterly Journal of the Royal Meteorological Society, p. e4940, https://doi.org/10.1002/qj.4940, 2025.

https://doi.org/10.5194/egusphere-2025-1212
Preprint. Discussion started: 25 March 2025

Hwang, Y.-T. and Frierson, D. M. W.: Link between the double-Intertropical Convergence Zone problem and cloud biases over the Southern Ocean, Proceedings of the National Academy of Sciences, 110, 4935–4940, https://doi.org/10.1073/pnas.1213302110, 2013.

Hájková, D. and Šácha, P.: Parameterized orographic gravity wave drag and dynamical effects in CMIP6 models, Climate Dynamics, https://doi.org/10.1007/s00382-023-07021-0, 2023.

Iles, C. E., Vautard, R., Strachan, J., Joussaume, S., Eggen, B. R., and Hewitt, C. D.: The benefits of increasing resolution in global and regional climate simulations for European climate extremes, Geoscientific Model Development, 13, 5583–5607, https://doi.org/10.5194/gmd-13-5583-2020, 2020.

Jeevanjee, N.: Vertical Velocity in the Gray Zone, Journal of Advances in Modeling Earth Systems, 9, 2304–2316, https://doi.org/https://doi.org/10.1002/2017MS001059, _eprint: https://agupubs.onlinelibrary.wiley.com/doi/pdf/10.1002/2017MS001059, 2017.

Jones, T. R. and Randall, D. A.: Quantifying the limits of convective parameterizations, Journal of Geophysical Research: Atmospheres, 116, https://doi.org/https://doi.org/10.1029/2010JD014913, 2011.

Kang, S. M., Held, I. M., Frierson, D. M. W., and Zhao, M.: The Response of the ITCZ to Extratropical Thermal Forcing: Idealized Slab-Ocean Experiments with a GCM, Journal of Climate, 21, 3521–3532, https://doi.org/10.1175/2007JCLI2146.1, 2008.

Kawai, H., Yoshida, K., Koshiro, T., and Yukimoto, S.: Importance of Minor-Looking Treatments in Global Climate Models, Journal of Advances in Modeling Earth Systems, 14, e2022MS003 128, https://doi.org/10.1029/2022MS003128, 2022.

Keil, P., Schmidt, H., Stevens, B., and Bao, J.: Variations of Tropical Lapse Rates in Climate Models and Their Implications for Upper-Tropospheric Warming, Journal of Climate, 34, 9747 – 9761, https://doi.org/https://doi.org/10.1175/JCLI-D-21-0196.1, place: Boston MA, USA Publisher: American Meteorological Society, 2021.

Lang, T., Naumann, A. K., Buehler, S. A., Stevens, B., Schmidt, H., and Aemisegger, F.: Sources of Uncertainty in Mid-Tropospheric Tropical Humidity in Global Storm-Resolving Simulations, Journal of Advances in Modeling Earth Systems, 15, e2022MS003 443, https://doi.org/https://doi.org/10.1029/2022MS003443, _eprint: https://agupubs.onlinelibrary.wiley.com/doi/pdf/10.1029/2022MS003443, 2023.

Lott, F. and Miller, M. J.: A new subgrid-scale orographic drag parametrization: Its formulation and testing, Quarterly Journal of the Royal Meteorological Society, 123, 101–127, https://doi.org/https://doi.org/10.1002/qj.49712353704, _eprint: https://rmets.onlinelibrary.wiley.com/doi/pdf/10.1002/qj.49712353704, 1997.

Ma, X., Zhao, S., Zhang, H., and Wang, W.: The double -ITCZ problem in CMIP6 and the influences of deep convection and model resolution, International Journal of Climatology, 43, 2369–2390, https://doi.org/10.1002/joc.7980, 2023.

Mauritsen, T., Stevens, B., Roeckner, E., Crueger, T., Esch, M., Giorgetta, M., Haak, H., Jungclaus, J., Klocke, D., Matei, D., Mikolajewicz, U., Notz, D., Pincus, R., Schmidt, H., and Tomassini, L.: Tuning the climate of a global model, Journal of Advances in Modeling Earth Systems, 4, 2012MS000 154, https://doi.org/10.1029/2012MS000154, 2012.

Morris, M., Kushner, P. J., Moore, G. W. K., and Mercan, O.: Resolution Dependence of Extreme Wind Speed Projections in the Great Lakes Region, Journal of Climate, 37, 3153–3171, https://doi.org/10.1175/JCLI-D-23-0547.1, 2024.

Müller, W., Lorenz, S., Pham, T. V., Schneidereit, A., Brovkin, V., Brüggemann, N., Chegini, F., Dommenget, D., Fröhlich, K., Früh, B., Gayler, V., Haak, H., Hagemann, S., Hanke, M., Ilyina, T., Jungclaus, J., Köhler, M., Korn, P., Kornblue, L., Kroll, C., Krüger, J., Niemeier, U., Potthast, R., Riddick, T., Pohlmann, H., Polkova, I., Schlund, M., Sgoff, C., Stacke, T., Wirth, R., and Yu, D.: Source

https://doi.org/10.5194/egusphere-2025-1212
Preprint. Discussion started: 25 March 2025

code and scripts for publication "The ICON-based coupled Earth System Model for Climate Predictions and Projections (ICON XPP)", https://doi.org/10.17617/3.UUIIZ8, artwork Size: 700, 95479689, 95510314 Pages: 700, 95479689, 95510314, 2024.

National Center for Atmospheric Research Staff, E.: The Climate Data Guide: OAFlux: Objectively Analyzed air-sea Fluxes for the global oceans, https://climatedataguide.ucar.edu/climate-data/oaflux-objectively-analyzed-air-sea-fluxes-global-oceans, 2022.

Niemeier, U., Wallis, S., Timmreck, C., Van Pham, T., and Von Savigny, C.: How the Hunga Tonga—Hunga Ha'apai Water Vapor Cloud Impacts Its Transport Through the Stratosphere: Dynamical and Radiative Effects, Geophysical Research Letters, 50, e2023GL106 482, https://doi.org/10.1029/2023GL106482, 2023.

Orr, A., Bechtold, P., Scinocca, J., Ern, M., and Janiskova, M.: Improved Middle Atmosphere Climate and Forecasts in the ECMWF Model through a Nonorographic Gravity Wave Drag Parameterization, Journal of Climate, 23, 5905 – 5926, https://doi.org/https://doi.org/10.1175/2010JCLI3490.1, place: Boston MA, USA Publisher: American Meteorological Society, 2010.

Paccini, L., Hohenegger, C., and Stevens, B.: Explicit versus Parameterized Convection in Response to the Atlantic Meridional Mode, Journal of Climate, 34, 3343–3354, https://doi.org/10.1175/JCLI-D-20-0224.1, 2021.

Pan, L. L., Honomichl, S. B., Kinnison, D. E., Abalos, M., Randel, W. J., Bergman, J. W., and Bian, J.: Transport of chemical tracers from the boundary layer to stratosphere associated with the dynamics of the Asian summer monsoon, Journal of Geophysical Research: Atmospheres, 121, https://doi.org/10.1002/2016JD025616, 2016.

Philander, S. G. H., Gu, D., Lambert, G., Li, T., Halpern, D., Lau, N.-C., and Pacanowski, R. C.: Why the ITCZ Is Mostly North of the Equator, Journal of Climate, 9, 2958–2972, https://doi.org/10.1175/1520-0442(1996)009<2958:WTIIMN>2.0.CO;2, 1996.

Prill, F., Reinert, D., and Zängl, G.: ICON Tutorial - Working with the ICON Model, https://doi.org/10.5676/DWD_pub/nwv/icon_tutorial2023, 2023.

Raschendorfer, M.: The new turbulence parameterization of LM, Tech. rep., Consortium for Small-Scale Modelling, http://www.cosmo-model.org, 2001.

Reick, C. H., Gayler, V., Goll, D., Hagemann, S., Heidkamp, M., Nabel, J. E. M. S., Raddatz, T., Roeckner, E., Schnur, R., and Wilkenskjeld, S.: JSBACH 3 - The land component of the MPI Earth System Model: documentation of version 3.2, p. 4990986, https://doi.org/10.17617/2.3279802, artwork Size: 4990986 Medium: application/pdf Publisher: MPI für Meteorologie Version Number: 1, 2021.

Ren, Z. and Zhou, T.: Understanding the alleviation of "Double-ITCZ" bias in CMIP6 models from the perspective of atmospheric energy balance, Climate Dynamics, https://doi.org/10.1007/s00382-024-07238-7, 2024.

Schmidt, H., Rast, S., Bao, J., Fang, S.-W., Jimenez-de la Cuesta, D., Keil, P., Kluft, L., Kroll, C., Lang, T., Niemeier, U., Schneidereit, A., Williams, A. I. L., and Stevens, B.: Effects of vertical grid spacing on the climate simulated in the ICON-Sapphire global storm-resolving model, EGUsphere, 2023, 1–34, https://doi.org/10.5194/egusphere-2023-1575, 2023.

Schneider, D. P., Deser, C., Fasullo, J., and Trenberth, K. E.: Climate Data Guide Spurs Discovery and Understanding, Eos, Transactions American Geophysical Union, 94, 121–122, https://doi.org/10.1002/2013EO130001, 2013.

Schneider, T., Bischoff, T., and Haug, G. H.: Migrations and dynamics of the intertropical convergence zone, Nature, 513, 45–53, https://doi.org/10.1038/nature13636, 2014.

Schneider, T., Leung, L. R., and Wills, R. C. J.: Opinion: Optimizing climate models with process knowledge, resolution, and artificial intelligence, Atmospheric Chemistry and Physics, 24, 7041–7062, https://doi.org/10.5194/acp-24-7041-2024, 2024.

https://doi.org/10.5194/egusphere-2025-1212
Preprint. Discussion started: 25 March 2025

Segura, H., Bayley, C., Fi´evet, R., Gloeckner, H., Guenther, M., Kluft, L., Naumann, A. K., Ortega, S., Sri Praturi, D., Rixen, M., Schmidt, H., Marius, W., Hohenegger, C., and Bjorn, S.: A single tropical rainbelt in global storm-resolving models: the role of surface heat fluxes over the warm pool, https://doi.org/10.22541/essoar.173482210.07670254/v1, 2024.

Seifert, A.: A revised cloud microphysical parameterization for COSMO-LME., http://www.cosmo-model.org, 2008.

Sherwood, S. C., Bony, S., and Dufresne, J.-L.: Spread in model climate sensitivity traced to atmospheric convective mixing, Nature, 505, 37–42, https://doi.org/10.1038/nature12829, 2014.

Si, W., Liu, H., Zhang, X., and Zhang, M.: Double Intertropical Convergence Zones in Coupled Ocean-Atmosphere Models: Progress in CMIP6, Geophysical Research Letters, 48, e2021GL094 779, https://doi.org/10.1029/2021GL094779, 2021.

Simmons, A., Soci, C., Nicolas, J., Bell, B., Berrisford, P., Dragani, R., Flemming, J., Haimberger, L., Healy, S., Hersbach, H., Horányi, A., Inness, A., Munoz-Sabater, J., Radu, R., and Schepers, D.: ERA5.1: Rerun of the Fifth generation of ECMWF atmospheric reanalyses of the global climate (2000-2006 only)., https://doi.org/10.24381/cds.143582cf, 2020.

Simpson, I. R., McKinnon, K. A., Kennedy, D., Lawrence, D. M., Lehner, F., and Seager, R.: Observed humidity trends in dry regions contradict climate models, Proceedings of the National Academy of Sciences, 121, e2302480 120, https://doi.org/10.1073/pnas.2302480120, 2024.

Song, X. and Zhang, G. J.: The Roles of Convection Parameterization in the Formation of Double ITCZ Syndrome in the NCAR CESM: I. Atmospheric Processes, Journal of Advances in Modeling Earth Systems, 10, 842–866, https://doi.org/10.1002/2017MS001191, 2018.

Takasuka, D., Kodama, C., Suematsu, T., Ohno, T., Yamada, Y., Seiki, T., Yashiro, H., Nakano, M., Miura, H., Noda, A. T., Nasuno, T., Miyakawa, T., and Masunaga, R.: How Can We Improve the Seamless Representation of Climatological Statistics and Weather Toward Reliable Global K-Scale Climate Simulations?, Journal of Advances in Modeling Earth Systems, 16, e2023MS003 701, https://doi.org/10.1029/2023MS003701, 2024.

Tan, Z., Kaul, C. M., Pressel, K. G., Cohen, Y., Schneider, T., and Teixeira, J.: An Extended Eddy-Diffusivity Mass-Flux Scheme for Unified Representation of Subgrid-Scale Turbulence and Convection, Journal of Advances in Modeling Earth Systems, 10, 770–800, https://doi.org/10.1002/2017MS001162, 2018.

Tian, B. and Dong, X.: The Double-ITCZ Bias in CMIP3, CMIP5, and CMIP6 Models Based on Annual Mean Precipitation, Geophysical Research Letters 28 April 2020 47(8): e2020GL087232, num Pages: - e2020GL087232, 2020.

Tian, B., Fetzer, E. J., and Teixeira, J.: Assessing the Tropospheric Temperature and Humidity Simulations in CMIP3/5/6 Models Using the AIRS Obs4MIPs V2.1 Data, Journal of Geophysical Research: Atmospheres, 129, e2023JD040 536, https://doi.org/10.1029/2023JD040536, 2024.

Tiedtke, M.: A Comprehensive Mass Flux Scheme for Cumulus Parameterization in Large-Scale Models, Monthly Weather Review, 117, 1779 – 1800, https://doi.org/https://doi.org/10.1175/1520-0493(1989)117<1779:ACMFSF>2.0.CO;2, place: Boston MA, USA Publisher: American Meteorological Society, 1989.

Wild, M.: The global energy balance as represented in CMIP6 climate models, Climate Dynamics, 55, 553–577, https://doi.org/10.1007/s00382-020-05282-7, 2020.

Yu, L. and Weller, R. A.: Objectively Analyzed Air–Sea Heat Fluxes for the Global Ice-Free Oceans (1981–2005), Bulletin of the American Meteorological Society, 88, 527–540, https://doi.org/10.1175/BAMS-88-4-527, 2007.

Zhang, C.: Double ITCZs, Journal of Geophysical Research: Atmospheres, 106, 11 785–11 792, https://doi.org/10.1029/2001JD900046, 2001.

https://doi.org/10.5194/egusphere-2025-1212
Preprint. Discussion started: 25 March 2025

Zhang, H., Deser, C., Clement, A., and Tomas, R.: Equatorial signatures of the Pacific Meridional Modes: Dependence on mean climate state, Geophysical Research Letters, 41, 568–574, https://doi.org/10.1002/2013GL058842, 2014.

Zhang, Y. and Boos, W. R.: An upper bound for extreme temperatures over midlatitude land, Proceedings of the National Academy of Sciences, 120, e2215278 120, https://doi.org/10.1073/pnas.2215278120, 2023.

Zhou, W., Leung, L. R., and Lu, J.: Linking Large-Scale Double-ITCZ Bias to Local-Scale Drizzling Bias in Climate Models, Journal of Climate, 35, 7965 – 7979, https://doi.org/https://doi.org/10.1175/JCLI-D-22-0336.1, place: Boston MA, USA Publisher: American Meteorological Society, 2022.

Zängl, G., Reinert, D., Rípodas, P., and Baldauf, M.: The ICON (ICOsahedral Non-hydrostatic) modelling framework of DWD and MPI-M: Description of the non-hydrostatic dynamical core, Quarterly Journal of the Royal Meteorological Society, 141, 563–579, https://doi.org/https://doi.org/10.1002/qj.2378, _eprint: https://rmets.onlinelibrary.wiley.com/doi/pdf/10.1002/qj.2378, 2015.